MECHANISMS OF COMPOSITE SOLID PROPELLANT COMBUSTION

Final Report

Naval Weapons Center, China Lake, California

Contract #N00123-72-C-0242

Warren C. Strahle

John C. Handley

Thomas T. Milkie

Georgia Institute of Technology

School of Aerospace Engineering

Atlanta, Georgia 30332

ABSTRACT

Results are presented of an experimental-theoretical program involving sandwich combustion of compacted polycrystalline AP; binders of HTPB, CTPB, polyurethane, and PBAA; and iron oxide and copper chromite catalysts. Exploratory studies of sandwich behavior with aluminum addition to the binder and the use of ammonium nitrate and potassium perchlorate oxidizers are also presented. The pressure range covered is 600-3200 psia, and the experimental technique of cinephotomacrography is used. An integral method is applied to the analytical problem of sandwich combustion, and, while not entirely successful, several important order of magnitude arguments and relationships which must hold at the binder-oxidizer interface are presented. The importance of sandwich studies in interpretation of real propellant behavior is elucidated. The primary results are that a) in the pressure range studied the binder-oxidizer interaction for uncatalyzed situations take place on a size scale of interest in real propellants and is most probably dominated by melt rather than chemical behavior and b) other than catalysis of the AP deflagration a primary effect of catalysts occurs near the binder oxidizer interface. Further experiments are required to determine the exact nature of this interface behavior.

TABLE OF CONTENTS

NOMENCLATURE

b	Pyrolysis constant
c_p	Heat capacity of gas phase (at constant pressure)
c_s	Heat capacity of solid phase
E	Activation energy
f	Distribution of gas phase temperature of Eq. (22)
g	Dimensionless temperature
n, s	Coordinates
p	Pressure
q	Dimensionless phase transition (+ if endothermic) or gas phase heat release, $\frac{q^*}{c_p T_o}$ (+ if exothermic)
$\dot{q}$	Dimensional heat release rate per unit volume
R	Universal gas constant
Re	Reynolds number
r	Burn rate
$\dot{r}_{AV}$	Experimental average vertical regression rate
$r_{AV} \cos \theta$	Experimental average regression rate normal to the surface on the AP surface away from the binder
T	Temperature
v	Vertical velocity of gas phase
x, y	Cartesian coordinates
Y	Mass fraction
z	$\sqrt{1 + (dy_s/dx)^2}$
α	Thermal diffusivity (or see below)
α, β	Constants due to f distribution

δ	Thickness
ϵ	Dimensionless activation energy, E/RT_o
η	c_s/c_p
θ	Angle between the surface parallel and the horizontal
$\varkappa$	Curvature, $(d^2y_s/dx^2)/[1 + (dy_s/dx)^2]^{3/2}$
λ	Thermal conductivity
ξ	$\lambda_s c_p/\lambda_g c_s$
ρ	Density
τ_r	Reaction time

SUBSCRIPTS

AP	Ammonium perchlorate
f	Flame
F	Fuel or NH_3 in the case of AP deflagration
g	Gas
s	Solid phase or gas-solid interface
o	Cold "soak" temperature
v	Vertical

SUPERSCRIPTS

*	Dimensional quantity
'	Differentiation with respect to x
$\rightarrow$	Vector quantity

I. INTRODUCTION

Rocket motor applications impose demands for a variety of burning rate characteristics of solid propellants, the attainment of which is usually achieved by costly means and with significant compromise in other performance attributes. Research has revealed a qualitative understanding of propellant combustion, and it is clear that the exothermic reactions that sustain the combustion may occur in varying degrees in the gas phase, on the burning surface, or in the condensed phase. The relative importance of the different reaction steps differs according to the composition of the propellant, details of the microstructure of the propellant, and environmental conditions. In most practical combustion situations we do not know the relative importance of these steps in the combustion zone, and the predictive capability we have is largely based on experience rather than theory. Since the relative importance of the competing processes in the combustion zone is unknown, no adequate analytical model exists as a predictive tool for a wide variety of practical combustion situations. The failure of analytical models is enhanced by the lack of fundamental kinetics data for binder and oxidizer decomposition, gas phase reactions, catalytic reactions, and interface reactions.

An extreme difficulty facing experimenters in this field has been that of observation of the combustion details in the three-dimensional environment of composite solid propellants. As a compromise between the complexity of real three-dimensional propellants and the retention of some heterogeneous structure, several workers have investigated two-dimensional sandwiches of oxidizer and binder (1-7). The studies of Ref. 4, restricted to PBAA binder and AP oxidizer and to a pressure range between 100 and 1200 psia, led to a number of significant discoveries such as: a) the presence of a stable surface pattern with a decomposing melt on the surface of ammonium

perchlorate, b) the absence of significant interfacial reactions between AP and binders in the condensed phase part of the combustion zone, and c) determination of the temperature of the solid surface of the AP during burning.

Nadaud (1) burned sandwich-like samples consisting of two slabs of polybutadiene pressed against a slab of AP. Various bonding agents between the AP and polybutadiene were tested and the results showed that interfacial propagation during combustion depended greatly upon the bonding method used. Actual tests were then run using no bonding agents, but with two slabs of polybutadiene tightly pressed against a slab of AP. Polyurethane was also used as a fuel. The results indicate that in the pressure domain from atmospheric to 300 psi Fenn's theory (8) provides a reasonable representation of the state of affairs. The leading edge of the regressing surface was noted to be at the interface between the AP and the fuel. This statement, however, is misleading in the light of other work; the photographic resolution was insufficient to tell whether or not the maximum regression was occurring exactly at the interface. This interface regression result is contradictory to the results of Refs. (4) and (5). Although the leading edge of the regressing surface is often near the interface, it is always displaced into the oxidizer.

In perhaps the most extensive sandwich work dealing with interfacial details, Varney (5) investigated rapid depressurization quenched samples by a unique silicone replica technique and photomicroscopy. The binders polysulfide (PS), polyurethane (PU), polybutadiene acrylic acid (PBAA), and carboxy terminated polybutadiene (CTPB) were used. The pressure range 300-2400 psig was spanned. Compacted polycrystalline AP was used, since Boggs (9) was able to verify that the samples prepared in this laboratory matched single crystal deflagration rates, and the pressed sample results

showed no apparent difference in quenched surface profile between pressed AP sandwiches and samples made with single crystal AP. Significant conclusions were a) there was no evidence of interfacial reactions between the binder and oxidizer at any pressure or with any binder, and b) all four of the binders exhibited a melt regardless of the pressure. Because of uncertainties in the flame structure and location, in the sandwich regression history and in the potential ejection of the binder in the quench process, Varney concluded that it was imperative that high speed motion picutres be taken of the sandwich combustion process.

Jones (6) has carried out cinephotomacrography studies of the same sandwich configurations studied by Varney with the addition of copper chromite (CC) and iron (III) oxide (IO) runs at 600 and 2000 psi. The sandwich technique using compacted polycrystalline AP is a unique vehicle for sandwich studies because of the variety of ways in which the catalyst may be added. From careful analysis of surface profiles and burn rates it was concluded by Jones that with these two catalysts only gas phase catalytic mechanisms are possible, using CTPB binder. Postulates of Pearson (10) and Pearson and Sutton (11) concerning catalytic decomposition of the binder are of doubtful validity. Motion picture resolution was insufficient, however, to determine whether or not the maximum point of sandwich regression takes place precisely at the binder-oxidizer interface, in catalyzed situations.

Jones's motion picture work was also valuable in removing some of the uncertainties introduced by quench testing such as a) the attainment of a steady state, b) the role of the binder melt, c) the flame location, d) the origin of asymmetric profiles, and e) the possible ejection of sandwich material during the quench process. Jones found that indeed part of the binder, protruding above the mean surface, was being ejected. The binder

melt observed by Varney does change the flame structure for PBAA, CTPB, and PU binders by moving the mean flame surface above the AP. In the case of PS, however, the melt does not appear to flow onto the AP. Jones found that a steady state is indeed attained and that asymmetries only develop from asymmetric ignition, local unsteadiness, or sandwich flaws.

Concurrent with the work of Varney and Jones, Boggs and Zurn (7) conducted studies using crystal AP and CTPB, HTPB, and PU sandwiches. Motion picture studies were made over the pressure range 100-1000 psia. Significant conclusions were that a) there was no evidence of interfacial reaction, in concurrence with Varney's findings, b) all binders displayed a melt, and c) the flame structure was rough, in that "the CTPB and HTPB propellants burned with many spatially and temporally unsteady flamelets...." This instability, which has been called "turbulence" in Ref. (7), using support from Ref. (12), is more properly ascribable to binder melt behavior than to a fluid mechanical instability of the gas phase.

It has been recognized by workers in this field that a barrier to the interpretation of the experimental results has been the lack of an analytical model of the sandwich problem. It is extremely difficult to reason concerning the heat and mass transport processes in a two-dimensional sandwich problem, considering the several competing processes and the complication of a two-dimensional surface. There has previously been only one treatment of the sandwich problem (13), but so much of the physics, chemistry, and surface structure detail were omitted to render the mathematics tractable that the model is useless in interpretation of sandwich details. One purpose, therefore, of the program reported here, was to make progress in development of an analytical model which would be useful in interpreting experimental results. Ideally, the processes which should be considered are a) the two-dimensional solid and gas phases fluid mechanics and transport phenomena,

b) a full model for AP deflagration, c) the chemistry of binder pyrolysis, d) the chemical kinetics of the AP deflagration, reactions between the AP deflagration products and binder pyrolysis products, and reactions between the AP decomposition products and pyrolysis products, e) the chemistry modifications of catalysts as well as any potential interface reactions, and f) the effects of binder melts. Obviously, treatment of all of these effects would present a formidable task. An initial attempt at model development is described in this report.

The objectives of the experimental program presented herein were to: a) catalogue through cinephotomacrography the PU, PBAA, CTPB, and HTPB binder regression histories as a function of pressure over the range 600-3200 psia, b) investigate catalyst behavior with AP-HTPB sandwiches over the same pressure range with copper chromite (CC) and iron (III) oxide (IO) catalysts, and c) determine the usefulness of cinephotomacrography for sandwich studies using aluminum in the binder and using oxidizers other than AP.

The pressure-binder catalogue was to expand upon the work of Jones, who investigated polysulfide over the same pressure range. The catalytic work was also to expand upon Jones's work, which used CTPB binder and only investigated the pressures 600 psia and 2000 psia. The majority of work used HTPB binder, as a more advanced binder than CTPB.

II. CINEPHOTOMACROGRAPHY EXPERIMENTS

A. Instrumentation, Equipment, and Procedures

The techniques and equipment used were basically that described by Jones (6). However, since there were some modifications in the current program and Jones's description is not in the readily accessible archive literature as yet, some detail will be given here concerning the experiment mechanics.

The experimental investigation was conducted in the Georgia Institute of Technology Aerospace Engineering Propulsion Laboratory. Principal aspects of the facility are a high pressure, variable flow combustion vessel equipped for photography, a high speed movie camera, a high intensity light source, a motion analyzer (movie projector), and associated laboratory apparatus required for sample preparation and data analysis.

The combustion facility consists of a nitrogen supply, an orifice for flow measurement, a window bomb in which the sample was ignited and miscellaneous valves, plumbing, gauges, and controls.

Nitrogen was supplied to the combustion vessel from two high pressure cylinders. One or two cylinders were used depending on the flow requirements. Burning rates were determined at combustion vessel pressures, up to 3200 psia. High pressure nitrogen cylinders were used along with tank valves for 6000 psig service. The tanks were filled locally with 494 standard cubic feet of nitrogen at 6000 psi.

The two nitrogen cylinders were connected to a three-station, single row brass manifold supplied by the Matheson Company. The manifold, rated for 6000 psig safe working pressure, was mounted on the combustion system enclosure wall.

The nitrogen was admitted to the system from the manifold through the System Supply Valve, a Hoke Roto-Ball, type 303 stainless steel valve (P/N 7223F85). This type valve was also used as the Safety Vent Valve which provided a nitrogen bleed capability in case of a regulator lock-up or other unforeseen difficulty in the pressurization system.

Manifold supply pressure was monitored on a Marsh type 210 pressure gauge. This gauge is constructed of type 403 stainless steel and has a pressure range of zero to 8000 psig. Accuracy was ± 20 psi and readability was 50 psi.

Nitrogen flow was monitored using a sharp-edged flow orifice furnished by Vickery-Simms, Inc. The orifice meter tube assembly rated at ASA 1500# and was made of type 316 stainless steel. Schedule 80, 3/4 inch pipe was used upstream and downstream of the orifice plate. The orifice plate is 1/8 inch thick and the orifice hole is 0.136 inches in diameter. The orifice meter tube assembly and the orifice plate conform to guidelines laid down by the ASME and by the American Gas Association.

The pressure drop across the orifice was measured using a zero to 100 psi ΔP gauge furnished by the ITT Barton Company. This gauge is a Barton Model 227 made of type 316 stainless steel and rated at 6000 psig SWP. Accuracy is ± 0.5 psi and readability is 1 psi.

Since new high pressure nitrogen tanks were used for this investigation, the nitrogen pressure regulator was moved to the upstream side of the flow metering orifice. This permitted the tests to be carried out with a constant nitrogen flow velocity.

The nitrogen pressure was maintained constant during the run by a Victor Controls dome-loaded pressure regulator, Model GD 68. The Model GD 68, a diaphragm operated, balanced poppet regulator with type 316 stainless steel body and springs and "Viton" diaphragm and seals is rated for

10,000 psig service. This regulator was in turn controlled by a Victor Controls LR series pressure reducing regulator which maintained the proper dome loading for the Model GD 68. The LR series regulator is a low flow, high pressure regulator for the control of pressure up to 10,000 psig. The LR regulator is self-relieving and has a hand wheel control.

Combustion pressure was monitored by a Marsh type 210 pressure gauge. This gauge is constructed of type 403 stainless steel and has a pressure range of zero to 5000 psig. Accuracy is ± 12.5 psi and readability is 20 psi.

A stainless steel pressure vessel equipped for photography was used for control of the combustion atmosphere. The combustion vessel is a three piece assembly with provisions for sample ignition, lighting, and photography:

1. The lower section provides an inlet for the nitrogen pressurization flow, houses the ignition circuitry, and serves as a base for the sample holder assembly.

2. The center section serves as the combustion section and has quartz windows for lighting and photography. The windows are ground and polished General Electric Type 151 Clear Fused Quartz Discs, 1 1/2 inches in diameter and one inch thick.

3. The top section provided an exit for the exhaust flow. The three piece combustion vessel is retained by upper and lower stainless steel, threaded collar rings on the O.D. of the combustion section and utilizes rubber "O"-rings for leak proof pressure control.

The sample holder assembly is attached to the lower section of the combustion vessel and serves three functions:

1. Provides a means for sample support in the combustion section.

2. Initiates smooth flow past the combustion sample via a five micron, sintered stainless steel porous plate which serves as the floor of the holder assembly.

3. Provides an extension of the ignition circuitry to the proximity of the combustion sample.

Sample ignition was accomplished by electrically heating a single strand of 10 mil nichrome wire positioned on the upper sandwich surface. The wire was positioned such that it would not interfere with the photography and also such that it lay along the binder layer. A drop of Goodyear plioband rubber cement was applied to the ignition wire and the top of the sample. The ignition power was supplied by an 18 volt D.C. power supply. The ignition of the sample was accomplished by starting the high speed camera. Using the camera speed curves included in Jones's work, the number of feet of film exposed before the camera reached full speed could be determined. An event microswitch located in the camera was adjusted to close when that footage of film had been exposed. This switch completed the electrical circuit for the ignition of the sample.

Smooth regulation of the combustion vessel purge flow was provided by a Hoke 270 series needle valve in the exhaust portion of the flow system.

Nitrogen flow lines were constructed of type 316 stainless steel tubing having either a 3/4 inch O.D. with a 0.120 inch wall thickness or a 1/4 inch O.D. with a 0.049 inch wall thickness and with type 304 stainless steel tubing having either a 3/4 inch O.D. with a 0.109 inch wall thickness or a 1/4 inch O.D. with a 0.049 inch wall thickness. Leak-proof connections were made using Crawford "Swagelok" type 316 stainless steel tube fittings.

High speed photography of the combustion of the sandwiches was accomplished with a Hycam 16 mm high speed motion picutre camera, Model K 20S4E-115. This camera was supplied by Red Lake Laboratories, Inc. and has a film capacity of 400 feet of standard thickness film on daylite spools. The frame rate is variable from 10 to 11,000 pictures per second.

The Hycam camera was mounted on a table which was supported by three threaded rods with leveling feet and locking nuts which permit the camera height to be adjusted or the entire camera to be tilted. This table was attached to a Palmgren No. 83 Rotary Table with Cross Slides which has adjustments for movement of the camera perpendicular and parallel to the sample as well as rotary motion in a horizontal plane. The rotary table was in turn mounted on a six foot Sheldon Machine Company lathe bed along with the combustion vessel. The combustion vessel was fixed in place on the lathe bed while the camera was free to slide perpendicularly to the combustion vessel and then be secured at the desired location.

Special features of the Hycam camera are a remote ON/OFF switch, a ground glass focusing gate, an event synchronizer, and film speed timing lights. The ground glass focusing gate was used for critical focusing. It was placed in the location of the regular focusing gate during camera set-up and then removed for the actual filming process. The event synchronizer allowed the camera operator to either start or stop an event when a pre-set amount of film had been used. This was used to close the ignition circuitry during a run. The camera contains dual timing lights. One timing light was used for determining film speed. The light used for timing was driven by a Red Lake Timing Light Generator, Milli-Mite Model TLG-3. This generator flashes the timing light at 10, 100, or 1000 cps. The light left marks along the side of the film, thus allowing accurate film speed to be determined. Due to an instability noted in the timing frequency, a counter was used to note the frequency at the start and finish of a run.

The camera was equipped with an 85 mm, f/1.8 Vivitar Preset Lens. This lens along with a lens reversing adapter and proper extension tubes was used for magnifications of the samples from 1:1 to 2:1.

As an aid in determining proper exposures a Honeywell Pentax 1°/21° Exposure Meter was available. This meter could be used for either "spot" or "average" light meter readings. The meter calculator for this meter was specifically set up for use with the Hycam camera, with pictures per second rather than shutter speed marked on the calculator.

The sample magnification was determined by placing a small 1/64 inch scale on the sample holder and varying the total length of the extension tubes until the proper number of marks were visible on the camera's ground glass. The depth of field was extremely shallow when the image was magnified at 2:1. Therefore, accurate focusing was imperative. There was definite movement of the sample holder as the combustion vessel was pressurized. Several attempts were made to minimize this movement, but they were not completely successful. By focusing at atmospheric pressure and recording the camera movement necessary to refocus at higher pressures, it was possible to obtain a correction factor for the initial focus position.

High intensity illumination of the sample was available through the use of a XeTron 2500 watt xenon lamp system. The system consists of a power supply, a lamphouse, and a lamp.

The power supply is a XeTron solid state power supply, Model N3-X95/140DM. This power supply requires 220 volt, 3 phase, 60 cycle A.C. input and delivers 28-40 volts D.C. at 75-140 amps output. This provided power to ignite the lamp initially as well as power to sustain the illumination.

The lamphouse is a XeTron Model 4000X, Type 25. The lamphouse contains mirrors for directing the light and holding the xenon lamp. Controls for focusing the light and moving it horizontally or vertically were in the lamphouse. The lamp housing was equipped with a shutter to prevent unnecessary sample illumination.

Both the power supply and the lamphouse are capable of using a 4000 watt xenon lamp. However, a 2500 watt xenon lamp was used in this study. This lamp is an Osram XBO 2500W lamp, and it was operated at a mean D.C. voltage of 30 volts, a minimum current of 60 amps and a maximum current of 95 amps. Light from this lamp had practically the same spectral properties as daylight composed of mixed direct sunlight and indirect light from the sky. Therefore, no color correction filter was needed for color photography when using daylight type film.

Cooling for the lamp was provided by a Grainger 7C037 Blower. Air at a rate of 300 cfm flowed through a filter in the base of the lamphouse, past the lamp, and then out the top of the lamphouse into a flexible hose connected to the blower. The blower then exhausted the air into the laboratory.

In order to prevent unwanted infrared radiation from entering the combustion vessel an infrared absorbing, visible transmitting filter was installed over the illumination window of the combustion vessel. This filter was a Corning CS 1-75, two inches square.

Heavy glass mortars and pestles were used to thoroughly grind crystalline AP into a fine powder. AP polycrystalline compaction was achieved using a six piece mold in a Carver Laboratory Hydraulic Press.

All precision weighings required in sample formulation were made using a Mettler H6T Digital Balance. The Mettler H6T is a single pan, beam balance using synthetic sapphire knife-edged bearing planes for beam support. Weight compensation was accomplished by a combination of built-in ring weights. Readout was in digital form and was read optically. The weighing range of the H6T was zero to 160 grams with a standard deviation precision of ± 0.05 milligrams.

Binder samples were cured in an Acme Laboratory Vacuum Oven, Model 43573, which has a temperature range of 35-260 °C maintained within ± 1°C

of the selected level. Vacuum conditions in excess of 28 inches of mercury were provided by a Welch two-stage Duo-Seal vacuum pump driven by a Craftsman one-half horsepower electric motor.

Microscopic determination of the sandwich binder thickness was achieved using a Bausch and Lomb Dynazoom Laboratory Microscope. The microscope permits fixed magnifications ranging from 40X to 1000X with a continuously variable 1X to 2X zoom magnification within each fixed setting. Basic illumination was achieved by a base mounted, variable output illuminator coupled with an Abbe condenser system. Photomicrographs can easily be made with the Dynazoom microscope which incorporates provisions for several camera assemblies. For this investigation a piece of ground glass with a marked scale on it was used at the film plane to determine binder thickness in microns. Adequate illumination to form the image on the ground glass required external illumination. A Fish-Schurman "Zirconarc" photomicrographic lamp and power supply were used to provide this external illumination. The "Zirconarc" is basically an arc lamp, with its electrodes fixed and sealed within a glass bulb containing an inert atmosphere. The power supply and lamp starter are a separate, self-enclosed unit operating from 110 volt A.C. power.

Propellant sandwiches were prepared from selected polycrystalline ammonium perchlorate (AP) discs. Certified grade ammonium perchlorate of 99.996% purity was supplied by Fisher Scientific Company. The crystalline AP was ground to a fine powder in a glass mortar and pestle (grinding time, approximately 10 minutes). It was found that 1.25 grams of the powdered AP would produce a 1 inch diameter disc that is .050 inch thick, when it was compacted under 22,000 psi. Compaction time varied from 8 to 24 hours.

When a catalyst was to be included in the AP discs, the correct proportions were weighed before grinding. Both the AP and the catalyst must be ground together. Separate mixing of the two fine powders is impossible

due to electrostatic repulsion. Improper mixing of the AP and catalyst will cause dark spots in the pressed disc. The mortar and pestle must be cleaned thoroughly after catalysts have been ground. It is preferable to use a separate mortar and pestle for each catalyst.

Catalysts were also mixed with the binders and painted on the AP-binder interface, using a paint of methyl-alcohol and the appropriate catalyst.

Binders were mixed in 30 ml plastic cups. A minimum of 5 grams of binder could be mixed up at a time due to the difficulty in measuring small quantities of the viscous constituents. After the binders had been mixed according to the formula, they were outgassed by placing the mixture in a glass bell jar and slowly reducing the pressure in the jar. Care must be taken to prevent violent foaming of the mixtures as it outgasses. All of the binders could be kept for 30 days if they were refrigerated. The mix used in all HTPB runs was

	Weight, %
R45M HTPB	90.428
IPDI	6.450
AO2246 antioxidant	0.980
MT-4 bonding agent	2.142

The mix for PU, PBAA, and CTPB was as reported by Jones.

The sandwiches were made using teflon shims to separate the discs and control the thickness of the binder. The teflon separator was used as a combination shim and mask. It was .005 inch thick and cut in a "U" shape. Both the double and triple sandwiches were assembled in a similar manner. With the shim in place on an AP disc, sufficient binder was placed on the disc to completely cover the disc to the desired thickness, with some excess. The second AP disc was then placed on this, and the process repeated if more layers were necessary. The completed sandwich was clamped together for

curing with several miniature alligator clips. These clips must be positioned over the portion of the sandwich supported by the shim material. The jaws of the clips were protected with small pieces of shrink tubing. The sandwiches were placed vertically in plastic cups, with the open section of the shim at the top of the sandwich. This prevented the binder from flowing out of the shim reservoir during the curing process.

At the end of the curing cycle, the oven was allowed to cool for at least two hours with the outer door open. Thermal shock can easily destroy the sample.

Once the sandwich reached room temperature the samples were cut to size. The outline of the teflon shim was scribed on the AP disc. Since the binder does not adhere to the teflon, it was removed by carefully pulling it out of the sandwich. The sandwich was then cut into six samples approximately 1 cm by 0.5 cm. A jeweler's saw with a .0075 inch thick blade and 40 teeth per inch was used. All edges of the samples were smoothed and squared using fine sandpaper and a razor blade. The finished sample was inspected, measured, and returned to the desiccator until it was ready to be tested. The binder thickness was measured with the microscope on 10X and the zoom magnification on 1X. Both the photomicrograph lamp and the microscope lower light were used to illuminate the sample.

Initial tests in this series were conducted using a nitrogen flow of one foot per second past the burning sample. This flow rate was determined by Jones, and it was necessary to remove the combustion products from the camera's field of view. In an attempt to stiffen the sample mounting post the inside diameter of the combustion vessel was increased from 1 to 1 1/4 inches. The volume flow rate was increased to again give a flow velocity of one foot per second. At that time sandwiches with catalysts in the binder were being tested. They were inherently smoky and gave much more

difficulty in obtaining good films due to recirculation of the smoke in the viewing windows. A more streamlined sample holder was constructed and the volume flow rate of nitrogen reduced to the values used in the original one inch diameter combustion vessel in order to obtain acceptable films.

The film from each run was viewed initially to determine the acceptability of the test. Sporadic or very fast burning tests caused by binder voids or flash burning down the front of the sample were rejected. The burning rate of the propellant was determined by projecting the film on to a sheet of graph paper with a total magnification of approximately 100X. The exact magnification was determined by comparing the image width with the micrometer-determined sample thickness. The sample image was aligned with the grid of the paper by moving the projector. Once the ignition transients had subsided, the projector was stoped and a sketch of the burning surface was made. The projector frame counter was reset to zero. The projector was restarted and allowed to run as long as the smoke flow and burning pattern allowed an unobstructed view of a well defined, burning edge. Another sketch was made of the burning edge before it disappeared from view. The two sketches were usually separated by approximately 200 frames. The initial and final angles of the burning edges were recorded. The vertical distance burned was measured close to the binder to avoid edge effects.

To determine the camera speed exactly, the film was rewound to the mid-point of the burning rate determination. The film was removed from the projector and placed on a light table, where a faint film timing mark that coincides with a sprocket perforation was located. A similar unique mark-perforation combination was located 2 to 3 feet away from the first pair. The intervening number of frames and timing marks was counted. By dividing the two integer values and multiplying by the recorded timing light counter average, a value of the camera speed was obtained.

B. Sandwich Mechanics

Shown in Fig. II-1 are the mechanics of data analysis used in this program. It has been verified by Jones and by the work of this program that, for binder widths of the order of 100 μ and overall sandwich widths of the order of 0.15 inch, the AP regresses as though it were self-deflagrating if it is observed sufficiently far from the binder-oxidizer interface, but away from the N_2 edge effects. Consequently, at point 1 in Fig. II-1-a the normal regression rate must be that of pure AP in the uncatalyzed case. It has also been verified, except in unusual cases to be identified later, that a steady state is always achieved at some time during the burn. Consequently, r_v is a constant. These facts have several important consequences such as: a) a sandwich cannot regress slower than pure AP, b) regions having higher inclination to the horizontal than θ_1 are regressing slower than pure AP normal to the surface, and c) a point of zero slope (point 2) has the maximum normal regression rate which is faster than for pure AP.

The eventual surface profile is most probably determined by the complex chemistry and physical processes in the region called the base flame of Fig. II-1-b. This is the ignition region for the diffusion flame which consumes the binder. Depending upon the physico-chemical details in this region, more fully discussed in Section III, the steady state surface profile adjusts to meet the above criteria. Consequently, if there were extremely fast kinetics in the base flame region and a large heat feedback, the region of maximum regression rate would probably occur near the binder-oxidizer interface. The sandwich profile would appear as in Fig. II-1-a. If the kinetics were slow or the binder were an excessively large heat sink or difficult to pyrolyze one might expect a "Christmas tree" profile with no point of zero slope. However, the edge effects caused by the N_2 will always cause an upslope near the edge and some point of zero slope will always occur.

It should be cautioned that the cinephotomacrography setup used here was of insufficient resolution to determine the actual point of maximum normal regression rate. In uncatalyzed cases, however, the inference from Varney's work is that the point of maximum regression always occurs into the oxidizer, as would be expected from the above model, because the binder is a heat sink. The best that can be said directly from the work here, however, is that often the point of maximum regression rate occurs near the interface, at least in catalyzed cases. No claim is made that the interface itself may be isolated.

C. Results

1. Binder-Pressure Studies

Figures II-2 through II-44 are prints from 16 mm motion picture frames for all successful runs made during the program. The actual color motion pictures may be obtained on loan from

Dr. Warren C. Strahle
School of Aerospace Engineering
Georgia Institute of Technology
Atlanta, Georgia 30332

Figures II-45 through II-50 are the burn rate results obtained in the program. For the binder-pressure studies Figs. II-2 through II-15 and II-45 and II-46 are pertinent.

Figure II-2 shows the general degree of two dimensionality achieved and gives an idea of the degree of roughness of the PU-AP flame. Figures II-2 through II-7 show PU behavior over the pressure range 300-3200 psia with omission at 1000 psia and 2400 psia, due to the work of Jones.

The PU behavior produces a quite flat AP surface over the entire pressure range, resulting in little separation of the AP burning rate ($\dot{r}\cos\theta$) and the sandwich burning rate ($\dot{r}$), as seen in Fig. II-45. There always appears at

some point in the run a leading edge binder melt as shown in Fig. II-4. In the case of Fig. II-3 the glossy substance on the right-hand sandwich face is a binder melt flow. The orange part of the flame is on average displaced from the interface onto the AP surface which strongly indicates that the effective location of the binder-oxidizer (BO) interface is displaced outward by a melt.

The flatness of the AP profile is, of course, the reason for very little separation of the open and blackened points on Fig. II-45. But this figure points out a difficulty which was encountered in the program. Ideally, the open points should follow the pure AP burn rate curve, as was found to be the case by Jones. Viewing Figs. II-45 and II-46, however, while the open points are consistent, regardless of the binder, the pure AP curve is not followed. Shown on the figures is the pure crystal AP burn rate curve when doped with 0.03 wt.% K^+.(7) Potassium contamination was suspected so a sample of the AP used in this program was sent to the Naval Weapons Center at China Lake for analysis; the result was that potassium was present at 0.03% by weight. This AP was from the same jar as used by Jones, and the source of contamination is a mystery. Because, however, the curves are consistent and the contamination was discovered late in the program, it was decided to continue the majority of testing with the contaminated AP. Some checks were made with runs with ultra-pure AP; these are described later.

The PBAA results are shown in Figs. II-3, 5, 6, and 7. Pressures excluded are 1000, 1500, and 2400 psia due to the work of Jones. The flame for PBAA is brighter and visibily more extensive than for PU. The majority of time during runs is spent with a reasonably flat AP profile. The "Christmas tree" profile does appear sporadically at 2000 psia as shown in Fig. II-5. Jones found flat profiles at 1000 and 1500 with a "Christmas tree" profile at 2400 psia. An exception to the flat profile is found at 2800 psia, but this

is due to an ignition transient effect in Fig. II-6. From the burn rate data of Fig. II-45 it may be seen that after a steady state was reached the AP was parallel with the horizontal. Coupled with the work of Jones, the melt behavior of PBAA is that the melts are as extensive but more viscous than with PU.

Figures II-8 through II-15 show the behavior of HTPB and CTPB sandwiches. With one exception the behavior of these two binders is almost identical. The flames are visibly more extensive than with PBAA; the leading edge melts are extensive and somewhat viscous, as with PBAA; the visible flames are definitely displaced over the AP, away from the binder; and the AP profiles are flat with the exception of "Christmas tree" profile development at 2400 psia.(Fig. II-13). The main exception appears to be a systematic increase in the AP burn rate if HTPB is used. The effect is mild ($\approx$ 20%) as seen in Fig. II-46 but appears systematic and outside of experimental error in burn rate determination ($\approx$ 10%). The only reasonable explanation for this phenomenon appears to be a mild radiation contribution from the BO flame to the AP heat input. This is plausible since the HTPB flame is slightly hotter than the CTPB flame.

With the exceptions of operation near the low pressure deflagration limit of AP and operation with binders producing a "Christmas tree" profile at 2400 and 2800 psig, these results, coupled with Refs. 5 and 6, indicate that the binder plays only a small role in the deflagration rate of sandwiches. Recall that the sandwich deflagration rate must be equal to or greater than that of pure AP regardless of whether the binder is a retardant or augmentor on the vertical rate near the interface. With pure binder-AP sandwiches if the chemical kinetics of the binder-AP flames were sufficiently fast, there should be a distinct leading edge of regression near the interface, and there is not. There should be a distinct separation of vertical

burn rate and AP burn rate producing a sharp upslope of the AP away from the interface, and this is not observed. The inescapable conclusions are that the kinetics are too slow, even at 3200 psia, to augment the sandwich rate or the binder melt flows inhibit regression near the interface. This is not inconsistent with previous remarks about inhibition causing a "Christmas tree" profile. The question is one of size scale. Varney's photographs show the "Christmas tree" in all cases within a limited distance of the binder. It is, in fact, difficult to imagine a process which would cause the extensive inhibition responsible for the "Christmas tree" profile of Fig. II-13. Since these always occur in a pressure regime characterized by an extensive needle-like surface structure of the AP (7), one wonders whether or not the AP itself is taking a major role in the formation of the profile of Fig. II-13. In Figs. II-5 and II-13 it might be noted that the binder chars are more extensive than in the other photographs. Whether or not this is significant is unknown.

With these motion picture results an extensive catalogue of behavior with PS, PU, PBAA, CTPB, and HTPB binders with compacted polycrystaline and pure crystal AP has been completed. The conclusions appear to be as mentioned above. With the exception of certain anomalous results and operation near the low pressure deflagration limit, the binder is a clear inhibitor to regression near the interface. Whether this is due to melt flows or slow chemical kinetics is unclear. Certainly an analytical model could shed some light here to give an idea of the size scales involved with each kind of inhibition and the detailed effects on surface shape.

2. Catalyst-Pressure Studies

Figures II-16 through II-29 show the results of HTPB-CC-AP sandwich studies and Figs. II-23 through II-36 show the corresponding results for IO catalyzed sandwiches. Three types of catalyst addition were employed:

a) 2% by weight pressed in with the AP alone, b) the same volumetric loading mixed in the binder alone, and c) a methyl alcohol paint of catalyst on the AP disc which was dried before applying the binder. These will be referred to as Types 1, 2, and 3, respectively.

From the result of this program that HTPB was highly similar in sandwich bheavior to CTPB in the uncatalyzed case, it was predicted that the catalysis results would be similar to Jones's work with CTPB-catalyst sandwiches. This indeed turned out to be the case. The main contribution here was better camera focus, especailly at high pressure and a more detailed pressure survey, in addition to the confirmation that CTPB and HTPB behaved similarly.

Triple sandwiches could only be used when there was no great disparity between the left and right-hand side regression rates. This generally meant that only below 1500 psia could triple sandwiches be employed except in the case of Type 2 sandwiches. It was found by Jones that each side of a double sandwich burned independently, there being little penetration effect across the binder. Consequently, when double sandwiches were burned, they were constructed of Type 1 one one side and Type 3 on the other side.

The burn rate results are shown in Figs. II-47 and II-48. The pure (contaminated) AP burn rate curve from the binder studies is superimposed on these figures. In the case of Types 2 and 3 catalyst addition the $\dot{r} \cos \theta$ points should line up on the pure AP burn rate curve, which they do fairly well. Especially with Type 3 sandwiches there is some difficulty in obtaining accurate cos θ values because of the high AP slope; consequently, the experimental error is larger here than with the pure binder studies.

With the darkening of the AP with catalyst in the Type 1 sandwiches, photographic lighting becomes a problem, and the figures are not as clear as with the pure binder studies. Conclusions have been drawn by detailed

observations of the motion pictures, but may not be apparent from the figures herein. Obviously, much detail is sacrificed by single frame, black-and-white, reproduced pictures as opposed to the actual motion pictures.

Evident in Figs. II-16 through II-22 is the fact that for both types 1 and 3 catalyst addition the vicinity of the interface always strongly leads the regression and the AP or CC-AP has a strong upslope away from the interface. Furthermore, there is no pressure level at which the "Christmas tree" profile occurs. Viewing Fig. II-47, except for a small dip near 2800 psi, the regression rate is uniformly augmented above the uncatalyzed case with a pressure increase for Type 1 addition. For Type 3 addition there is rate augmentation of a lower amount but which increases rapidly above 2000 psia until at 3200 psia the Types 1 and 3 have the same deflagration rate. Notice the extremely steep pure AP slope in Fig. II-21. These results clearly indicate that catalysis is most probably taking place in the gas phase for both the AP deflagration and BO flame. Until about 2000 psi the primary effect is catalysis of the AP deflagration rate. Above this pressure the rise of the Type 3 regression rate and the separation between $\dot{r}$ and $\dot{r}\cos\theta$ for Type 1 addition indicates an increased catalysis of the BO flame. These results are consistent with those of Jones. The possibility is not ruled out, however, of a heterogeneous attack upon the binder by catalyst-laden oxidizer gases in the vicinity of the interface.

Investigating Type 2 CC sandwiches in Figs. II-23 through II-29, there does appear to be a mild depression near the interface, but it is insufficient to augment the rate substantially as may be seen in Fig. II-47. Furthermore, the extent of the binder char is not altered as compared with Figs. II-8 through II-15. Thus, there appears no action upon the binder pyrolysis mechanism. It appears, therefore, that CC must get into the oxidizer laden gas phase before effect takes place. It may be mentioned

here that the Type 2 IO results are virtually identical with the CC results. It is interesting, however, that no "Christmas tree" profiles occur when the catalyst is added to the binder alone.

The IO results for Types 1 and 3 addition are shown in Figs. II-30 through II-36 and the IO burn rates are shown in Fig. II-48. The main comparisons to be made with CC and the primary observations are: a) IO inhibits the regression of AP itself until pressures above 1000 psi, in contrast to CC, b) at all pressures investigated some catalytic action is taking place near the BO interface and this action is greater than with CC at least until 2800 psia, as evidenced by the separation of $\dot{r}$ and $\dot{r}\cos\theta$ for Type 1 sandwiches and the same information from Type 3 sandwiches, c) at 2800 psi and above CC is superior to IO as a catalyst since it augments the BO reactions and AP deflagration rates in a superior manner, d) there is an interesting black residue deposited upon the AP surface with IO added in a Type 3 mode, particularly evident in Figs. II-30 and II-33, and e) there is an apparent depression of the AP rate ($\dot{r}\cos\theta$) with Type 3 addition at 600 psia, seen in Fig. II-47, which may be related to the residue.

Again, these more extensive results confirm the conclusions of Jones using the same catalysts with CTPB binder, except in one respect. This regards operation above 2000 psia, not investigated by Jones. At very high pressures addition of both catalysts to the interface (Type 3) produces maximum regression rates as fast as those achieved with addition to the AP (Type 1) for both catalysts. Thus, at sufficiently high pressure catalytic action in the vicinity of the interface appears as important as catalysis of the AP deflagration.

It is important that quench testing and detailed interface examination be performed in these catalyzed situations to determine whether action is taking place by gas phase attack upon the solid/liquid binder or whether the

action is taking place in the gas phase alone. Furthermore, the nature of the apparently sticky surface obtained with IO addition to the AP may be better examined.

The results of the sandwich work immediately suggest some conclusions/ predictions concerning actual propellant behavior, using these ingredients. The catalysts are not effective in the sandwich configuration when added to the binder, which is the conventional method of addition in propellants. The Type 3 results suggest that only by formation of a large surface area of AP, which is supplied in a real propellant by a fine oxidizer grind, or by delaying reaction a larger distance in the gas phase relative to the characteristic oxidizer size, also provided by small AP grind, can strong catalytic action take place, for a given volumetric loading of catalyst. Consequently, catalysts should become relatively more effective as the oxidizer grind becomes smaller. Furthermore, if a) ways could be found to coat the AP with catalyst and not allow it to become mixed with the binder and/or b) a method impregnating the AP with catalyst were employed the catalytic action would be more pronounced. The support for these contentions concerning actual propellants rests in the classified literature and cannot be discussed here.

3. Auxiliary Studies

This effort consisted of three brief studies: a) the usefulness of cinephotomacrography and sandwiches in the study of aluminum addition, b) the behavior of ammonium nitrate (AN) and potassium perchlorate (KP) oxidizers in the sandwich configuration, and c) the investigation of ultra-pure AP to hopefully check some results obtained with the contaminated AP.

Figures II-37 and II-38 show two triple sandwich runs with a) 50% Al in a 140 μ and 270 μ binder triple sandwich and b) 25% and 50% Al in 150 μ binders of a triple sandwich, respectively. The burn rate results are shown in Fig. II-49. Both Al tests were run at 1000 psia with a primary

objective to detect any surface agglomeration of the AP. Although the flame is brighter with the 50% aluminum addition as compared with the 25% addition, there is virtually no effect upon the burning rates as compared with AP alone, and the surface profiles are identical with that of Fig. II-9 (the left-hand side) for a pure HTPB-AP sandwich. More importantly, no agglomeration is discernible. It may be concluded that with this resolution cinephotomacrography with sandwiches is not a useful tool for investigation of Al behavior. This does not preclude, however, the sandwich usefullness if quench testing and high magnification photography are used.

Figures II-39 and II-40 show the AN-AP-KP sandwiches at 600 and 2000 psia, respectively. Difficulty was encountered in the manufacture of AN pressed pellets due to the hygroscopic nature of AN and in the ignition of the AN side of the sandwich. The highly mottled surface of the KP during the burn readily shows as a highly mobile melt in the motion pictures. It appears that the chemical kinetics of the BO flame are faster with KP than with AP because of the difficulty the center AP section has in following the regression at the KP-oxidizer interface. In these pictures a steady state was never achieved, because the KP does not self deflagrate. The flame structure was highly irregular making observation difficult. The 600 psia run of Fig. II-39 shows a regressing AN interface with no visible flame, but in Fig. II-40 AN ignition was never achieved. From the standpoint of manufacturing ease and interpretation of results, it is clear that AP in the sandwich configuration is far superior to the use of either AN or KP.

The most mysterious results of the program arose in the ultra-pure AP testing of Figs. II-41 through II-44 with the corresponding burn rate results of Figs. II-49 and II-50. Comparing Figs. II-8 and II-41 at 600 psia there is virtually no difference in surface profiles (as expected), but there is a significant depression in sandwich and AP burn rates in Fig. II-49 with

the ultra-pure AP. At 2000 psia, where a significant increase in burn rate for the ultra-pure AP was expected over the AP rate of the majority of tests, there was virtually no difference as seen in Fig. II-49. The surface profiles of Figs. II-12 and II-42 are highly similar also.

When the ultra-pure AP was catalyzed with IO in the Types 1 and 3 addition modes, the behavior of the two oxidizers was virtually identical except that Type 1 addition in the ultra-pure AP was more effective than in the test AP. The results suggest that the ultra-pure AP was also contaminated, but by what cause is unknown. A sample of the "ultra-pure" AP has been sent back to the Naval Weapons Center for analysis, but the results have not been available by the time the report was written.

III. ANALYSIS

A. Model Construction and Assumptions

Although a rudimentary picture of sandwich deflagration was presented in Section II-B, it would be desirable to have a reasonably complete analytical model to aid in experiment interpretation and to quantitatively establish the magnitudes of physico-chemical parameters required to produce observed effects. Even in the apparently benign two-dimensional configuration, however, the problem is highly complex due to a) an initially unknown surface shape, b) non-linearities in the equations due to chemical reaction and the unknown surface, c) two phase heat transfer, d) multiple chemical reactions, and e) a mathematically elliptic problem which reverts to a parabolic problem asymptotically away from the binder-oxidizer (BO) interface (as will become apparent later).

The maximum use of experimental information in the construction of the model is sought which does still not restrict the usefulness of the model in understanding experimental results. Accordingly, there have been several observations which have been used:

a) Far from the BO interface the AP regresses as pure AP and there appears little effect penetration across binder thicknesses of the order of 100 μ when dissimilar sandwiches are made. Consequently, the initial model development is concerned with a semi-infinite slab of AP against a semi-infinite slab of binder.

b) A steady state is achieved experimentally with AP oxidizer. Consequently, time dependence is assumed absent.

c) Viewed from the gas phase toward the solid phase, the surface is concave on average. This will influence the choice of coordinate system.

d) The experimental results indicate very little effect of the gas phase binder-oxidizer reactions upon the surface profile unless catalysts are employed.

Consequently, the initial model concerns itself with slow reactions (although the necessary magnitudes for these reactions to be important is investigated). Catalyst behavior is not investigated here.

Since a) above implies that a boundary condition far out on the oxidizer surface is a pure AP deflagration process, but the main purpose is to investigate the effects of the BO interface phenomena, a very simple AP model is employed. The Guirao-Williams (14) model is basically accepted which will limit the pressure range from 20-100 atm. This model will be slightly modified as outlined below. The concern is not with AP itself, and, in any event, there is no model accepted as yet above 100 atm. Actually the 100 atm upper limit is perhaps too severe and for qualitative sandwich analysis purposes the model is adequate to 2000 psia, where a distinctly different deflagration mechanism for AP appears. One of the major modifications is that a pyrolysis law will be used for the AP surface; whereas, it is generally accepted that the AP liquid-gas interface is in equilibrium (14). The reason for the present assumption is that it is computationally easier to treat and more readily yields certain BO interface relationships. While it is not believed that these will be strongly modified by an equilibrium assumption, there is as yet no proof; and a later investigation will treat the equilibrium case.

For the lack of any better information a simple pyrolysis law will be used for the binder solid (or liquid)-gas transition which is pressure independent. Furthermore, no effects of binder melts are considered in this initial treatment.

Other usual assumptions are made to simplify the analysis which, while they lead to numerical errors of order unity, do not alter significantly the scaling rules developed with respect to other variables. These assumptions are: a) the thermal and transport processes of the solid AP and binder are identical, b) the thermal and transport properties of all gas phase species

are identical, c) the Lewis number is everywhere unity in the gas phase, d) the deflagration process is a constant pressure process, e) heat conduction and mass transfer take place by temperature and concentration gradients only, respectively, and the transport coefficients are independent of temperature in both the solid and gas phases. A final major assumption is that on any vertical line parallel with the sandwich axis the ρv product in the gas phase is as determined at the gas solid interface and all lateral velocities are zero. This is in the spirit of the Burke-Schumann approximation as expounded in Ref. 15. This does yield error in convection effects upon heat transfer and in actual location of flames, but is too complex to treat here. The assumption may be relaxed by future analysis.

The configuration is shown in Fig. III-1, in which the coordinate system is rendered stationary by a translation of the interface in the y direction at the rate r. Under the stated assumptions the equations for solution and the boundary conditions are

Gas Phase

$$\lambda_g\left(\frac{\partial^2 T}{\partial x^{*2}} + \frac{\partial^2 T}{\partial y^{*2}}\right) = \rho v c_p \frac{\partial T}{\partial y^*} - \dot{q}^* \qquad (1)$$

Solid Phase

$$\lambda_s\left(\frac{\partial^2 T}{\partial x^{*2}} + \frac{\partial^2 T}{\partial y^{*2}}\right) = \rho_s r c_s \frac{\partial T}{\partial y^*} \qquad (2)$$

Boundary Conditions

$$T(y^* \to -\infty,\ x^* \text{ fixed}) = T_o$$

$$T(y^* \to \infty,\ x^* \to -\infty) = T_{AP_f}$$

$$T(y^* \text{ fixed},\ x^* \to \infty) = T_o$$

$$T(y^* \text{ fixed},\ x^* \to -\infty) = T_o \text{ if } \theta_{AP} < 0 \text{ or } = T_{AP_f} \text{ if } \theta_{AP} > 0$$

$$\vec{r}\cdot\vec{n})_F = b_F e^{-E_{sF}/RT_s(x^*)}$$

$$\vec{r}\cdot\vec{n})_{AP} = b_{AP} e^{-E_{sAP}/RT_s(x^*)}$$

$$\rho_s r = \rho(y^* = y_s^*(x^*),\ x^*)\ v(y^* = y_s^*(x^*),\ x^*)$$

$$-\lambda_g \frac{\partial T}{\partial n^*}\Big)_{s_g} = \rho_s r\ q_s^* - \lambda_s \frac{\partial T}{\partial n^*}\Big)_{s_s} \qquad (3)$$

T everywhere continuous

∇T continuous within a given phase

Equations (1) - (3) are incomplete in that $\dot{q}^*$, which accounts for heat generated by combustion, requires specification of mass fractions of all pertinent species, with attendant differential equations and boundary conditions required. For clarity of presentation and because of future developments these are omitted. The energy conservation condition of Eqs. (3) undergoes a discontinuity at $x = y = 0$ because q_s^* is discontinuous. Typical numbers used are

$T_o = 300^\circ K$	$\lambda_g = 2.0 \times 10^{-4}$ cal/cm°K sec
$\rho_s = 1.95$ gm/cm^3	$\lambda_s = 1.2 \times 10^{-3}$ cal/cm°K sec
$c_s = 0.275$ cal/gm°K	$c_p = 0.3$ cal/gm°K
$q_{s_{AP}}^* = -120$ cal/gm	$q_{s_F}^*$ is $\mathcal{O}[100 - 1000$ cal/gm$]$
$E_{s_{AP}} = 30{,}000$ cal/mole	E_{s_F} is $\mathcal{O}[3 - 6 \times 10^5$ cal/mole$]$

All heat of phase transition in the AP and the exothermic heat of transition to a liquid layer are included in $q_{s_{AP}}^*$, as well as the gasification heat. The orders of magnitude of $q_{s_F}^*$ and E_{s_F} are taken from the work of Varney.

B. Nondimensionalization of the Equations and the Characteristic Scales

The most convenient unit for length to take in the analysis is the one natural to Eq. (2). This is $\lambda_s/\rho_s c_s r = \alpha_s/r$, which contains the eigenvalue of the problem, r, the unknown sandwich regression rate. If r is near the regression rate of AP, then this length unit is known to be very close to the thermal wave depth in the solid AP. Taking 800 psia to be representative with $r_{AP} = 1.1$ cm/sec the characteristic length dimension has the magnitude

$$\alpha_s/r_{AP} = 2 \times 10^{-3} \text{ cm} = 20 \ \mu$$

Recall, however, that $r \geq r_{AP}$ so that the actual distance scale will be slightly smaller than the one computed using r_{AP}. The characteristic temperature chosen is T_o so that Eqs. (1) - (3) become, using $\rho_s r = \rho v$,

$$\underline{\text{Gas}} \qquad \frac{\partial^2 g}{\partial x^2} + \frac{\partial^2 g}{\partial y^2} = \xi \frac{\partial g}{\partial y} - \xi^2 \left(\frac{\dot{q}^*/\rho_g}{c_p T_o v}\right) \frac{\lambda_g}{\rho_g v c_p} \tag{4}$$

$$\underline{\text{Solid}} \qquad \frac{\partial^2 g}{\partial x^2} + \frac{\partial^2 g}{\partial y^2} = \frac{\partial g}{\partial y} \tag{5}$$

Boundary Conditions

$g(y \to -\infty, \text{ x fixed}) = 1$ $\qquad$ $g(y \to \infty, x \to -\infty) = g_{AP_f}$

$g(y \text{ fixed}, x \to \infty) = 1$ $\qquad$ $g(y \text{ fixed}, x \to -\infty) = 1$ if $\theta_{AP} < 0$

$= g_{AP_f}$ if $\theta_{AP} > 0$

$$\left(\frac{1}{z}\right)_F = \frac{b_F}{r} e^{-\epsilon_{s_F}/g_s} \qquad \left(\frac{1}{z}\right)_{AP} = \frac{b_{AP}}{r} e^{-\epsilon_{s_{AP}}/g_s}$$

$$\left(-\frac{\partial g}{\partial n}\right)_{s_g} = \xi\left[q_s - \eta \left(\frac{\partial g}{\partial n}\right)_s\right]$$

g everywhere continuous; ∇g continuous within a phase (6)

The parameter ξ in Eq. (4) is nothing more than the ratio of the characteristic solid phase dimension, α_s/r, to the characteristic gas phase dimension, α_g/v. Numerically $\xi = 6.55$, which indicates the first rather large disparity of characteristic dimensions which will be encountered. ξ would everywhere disappear from Eq. (4) if α_g/v were being used as the basic dimension rather than α_s/r. The significance of ξ is that, if other influences were absent, all important phenomena of heat transfer would take place in the gas phase in a region which has a characteristic (dimensionless) dimension of the order of $1/\xi$.

Now in Eq. (5) $\dot{q}^*/\rho_g$ is a heat release rate per unit mass in the gas phase and behaves like a heat release per unit mass divided by a reaction time. Thus,

$$\frac{\dot{q}^*/\rho_g}{c_p T_o v} = \left(\frac{q^*}{c_p T_o}\right) \frac{1}{\tau_r v}$$

which is a dimensionless heat release divided by a characteristic reaction distance in the gas phase. Consequently, the last term of Eq. (4) is of the same order of magnitude as the other terms only if

$$\frac{q^*}{c_p T_o} \left(\frac{1}{\tau_r v}\right) \text{ is } \mathcal{O}\left(\frac{\xi}{\alpha_s/r}\right)$$

that is, if the ratio of the characteristic heat transfer dimension is of the same order as the dimension required for chemical reaction. Consider, then, reactions between the binder and oxidizer, for which $q^*/c_p T_o \approx 11$. At 800 psi, $v \approx 165$ cm/sec so that unless

$$\tau_r \leq \frac{\alpha_s/r}{v\xi} \frac{q^*}{c_p T_o} = 2 \times 10^{-5} \text{ sec}$$

heat release due to reaction will not be important within a distance of the order of $1/\xi$ of the interface, where the dominant heat transfer processes are

occurring in the gas phase. As will be seen later, the pure AP flame is not this fast. Viewing the propane - O_2 data of Ref. 16, hydrocarbon oxidation times are only marginally this fast in the temperature environment seen here. Consequently, it appears that, in accord with experiments for uncatalyzed situations, the BO flame may not be important near the interface and only the heat transfer processes from the hot AP gases may be important in determining the details near the interface. Therefore, the initial model attempt will not consider BO reactions.

It will be seen later that the standoff distance of the AP deflagration flame is of the order of $2/\xi$ to $4/\xi$. Now the Reynolds number based upon vertical distance from the BO interface is

$$Re = \frac{\rho_g v y^*}{\mu} \approx \frac{\rho_g v y^*}{\lambda_g / c_p} = \xi y$$

Consequently, when y is $\mathcal{O}(1/\xi)$ there is the start of a transition from low to high Reynolds number flow. It is known from Ref. 17, and is reasonably obvious from experience with boundary layer flows, that Eq. (4) becomes of parabolic type as $Re \to \infty$. If this occurs, there is no influence of what happens at large y on small y events. Consequently, the interface is not influenced by what happens. Equations (4) and (5) are elliptic as they stand and every point in the field influences every other point, but this character will change at large y. The entire sandwich problem is therefore of mixed parabolic-elliptic type with only a region of the order of $1/\xi$ units thick in the gas phase influencing the interface.

Summarizing, the heat transfer processes in the solid phase take place one unit of thickness into the solid phase; the BO interface is influenced primarily by heat transfer from the reacting AP decomposition products; and at vertical distances where the AP deflagration is completed, the gas phase

problem has become parabolic in nature. The BO reactions may as a first approximation be neglected in the elliptic region for uncatalyzed cases.

C. The AP Flame

The pure AP flame forms a boundary condition at $x \to -\infty$ and must be treated. Following Culick's (18) procedure of assuming a flame standoff distance followed by instantaneous kinetics, a standoff distance determined by a reaction time of the form given by Guirao and Williams (14), and using the surface pyrolysis law mentioned in Eqs. (3) a solution to Eqs. (4) and (5) may easily be constructed. The only difficulty is with the assumption that the gas flow is vertical while the AP surface is inclined at θ_{AP}.

NH_3 and $HClO_4$ are considered as the decomposition products emanating from the liquid AP layer. For analytical purposes they are considered molecules of the same molecular weight. Since the reaction time is first order with respect to each of these species (16) a mass fraction equation must be added to Eq. (4). This is

$$\frac{\partial^2 Y_F}{\partial x^2} + \frac{\partial^2 Y_F}{\partial y^2} = \xi \frac{\partial Y_F}{\partial y} \tag{7}$$

with the boundary conditions

$$-\frac{\partial Y_F}{\partial n}\Big)_s = \frac{\xi}{z}\left(\tfrac{1}{2} - Y_{F_s}\right)$$

$$Y_F(n = n_f) = 0 \tag{8}$$

The solution to Eqs. (4), (5), and (7) subject to the appropriate boundary conditions is

Gas Phase

$$g - g_s = \left[q_{s_{AP}} + \eta(g_s - 1)\right] e^{-\xi/z_{AP}n} \qquad n \le n_f$$

$$Y_F = Y_{F_s} e^{-\xi/z_{AP}^n} + \tfrac{1}{2}(1 - e^{-\xi/z_{AP}^n}) \qquad n \le n_f$$

$$g_{AP_f} = g_s + q_{g_{AP}} - q_{s_{AP}} - \eta(g_s - 1) \tag{9}$$

Solid Phase

$$(g - 1) = (g_s - 1)\, e^{-n/z_{AP}} \tag{10}$$

Flame Standoff and Surface Condition

$$-n_f = \frac{z_{AP}}{\xi} \ln\left[\frac{q_{g_{AP}} - q_{s_{AP}} - \eta(g_s - 1)}{q_{s_{AP}} + \eta(g_s - 1)}\right] \tag{11}$$

$$y_f = -n_f z_{AP} \tag{12}$$

$$\tau_r = \frac{k_{AP}}{\rho Y_{F_s}^2} = \frac{y_f^*}{v} = \frac{y_f \alpha_s}{r^2}\left(\frac{\rho_g}{\rho_s}\right) \tag{13}$$

$$Y_{F_s} = \tfrac{1}{2}\left[1 - e^{\xi/z_{AP}^{n_f}}\right] \tag{14}$$

$$\frac{1}{z_{AP}} = \frac{b_{AP}}{r} e^{-\epsilon s_{AP}/g_s} \tag{15}$$

This model may now be forced to fit the AP burn rate curve by investigating the case of horizontal gas-solid interface where $z_{AP} = 1$ and $r = r_{AP}$. At 800 psia the surface temperature is assumed to be 800° k. From Eq. (15) b_{AP} is found to be 1.738×10^8 cm/sec. For an overall exothermicity of the AP deflagration of 320 cal/gm and the assumed $q_{s_{AP}}^* = -120$ cal/gm, $q_{g_{AP}}^* = 200$ cal/gm. Equation (11) then yields $-n_f = y_f = 2.34/\xi$ which forms the

basis for the previous remarks about the scale of the AP flame standoff. For $z_{AP} > 1$ the vertical standoff is larger because the vertical velocities are larger to accommodate the larger mass flow for a fixed horizontal area. From Eq. (14) $Y_{F_s} = .451$ and finally k_{AP} is calculated from Eq. (13) as $k_{AP} = 4.87 \times 10^{-5}$ sec atm. For any other surface temperature, r is calculated from Eq. (15), n_f from Eq. (11), Y_{F_s} from Eq. (14) and p from Eq. (13) yielding a unique pressure-burning rate curve which is known to match the experimental curve quite well (19), below 2000 psia.

In any sandwich model Eqs. (9) and (10) are boundary conditions on the temperature field far from the BO interface.

D. Surface and Interface Conditions and a Sandwich Paradox

From the pyrolysis conditions of Eqs. (6) an interesting set of relations arises. Differentiating, the curvature becomes

$$\varkappa = \frac{-g_s' \quad \epsilon_s}{\frac{dy_s}{dx} g_s^2} \tag{16}$$

Equation (16) relates the radius of curvature of the surface to the derivative of the surface temperature along the interface. In this relation the coordinate relation $dx/ds = 1/z$ has been used. Equation (16) requires that for the surface to be concave viewed from the gas that either a) g_s increases with s when $dy_s/dx < 0$ or b) g_s decreases with s when the surface slope is positive. All sandwiches viewed by Varney had positive slope and positive or near zero $\varkappa$ at the BO interface, and it may be concluded, assuming the pyrolysis law is valid, that the surface heat transfer along s is from the AP into the binder, as may be expected.

In the detailed interface photographs by Varney there was little evidence that the surface slope at the sandwich interface is discontinuous.

If, however, the binder and AP are undergoing independent pyrolysis laws, the temperature is continuous at the interface, and, of course, the vertical regression rate is the same for the binder and oxidizer, it may readily be shown that a continuous slope is impossible. This will be referred to as the "sandwich paradox."

The reason for this paradox lies in the behavior of the energy conservation law at the surface. It must be demanded by the Fourier conduction law that a unique, continuous heat transfer vector exists in the gas phase. This is shown in Fig. III-2. This heat transfer vector provides the heat of gasification of both the AP and binder at the interface. It must also be demanded that a unique heat transfer vector exists in the solid at the interface. Now in the AP the difference between $\vec{q}_g$ and $\vec{q}_s$ in the direction of $\vec{n}_{AP}$ goes toward providing the (negative) heat of gasification. The component parallel to the surface merely represents heat transport in the $\vec{s}$ direction at the surface. Similarly, the difference between $\vec{q}_{gas}$ and $\vec{q}_s$ in the direction of $\vec{n}_s$ must provide the (positive) heat of gasification of the binder. If $\vec{n}_s$ and $\vec{n}_{AP}$ were parallel (a continuous surface slope), an impossible situation would occur because the two heats of gasification are different. Consequently, the analytical model must allow a discontinuous slope.

Possible reasons for this apparent paradox are a) it is not possible to tell with the naked eye whether or not there is truly a continuous slope in Varney's photographs, b) a post quench binder melt run obscures the actual burning configuration, c) the possibility exists of heterogeneous attack on either the binder or oxidizer (they do not pyrolyze independently), or d) the assumption of equilibrium at the AP-gas interface may alter the the above reasoning. The last reason will be investigated in future work. Presently, however, it will be accepted on theoretical grounds that the slope must be discontinuous.

If it is presumed that along the $\vec{n}_{AP}$ line the temperature profile looks like

$$g - 1 = (g_s - 1)\ e^{-n/\delta_{AP}} \tag{17}$$

and along the $\vec{n}_F$ line

$$g - 1 = (g_s - 1)\ e^{-n/\delta_F} \tag{18}$$

then an exact solution to Eq. (5) may be found. Assuming

$$(g - 1) = (g_s - 1)\ e^{-\alpha x} e^{\beta y} \tag{19}$$

in Eq. (5) yields the condition that

$$\alpha^2 + \beta^2 = \beta \ ; \ \alpha \text{ and } \beta \text{ positive} \tag{20}$$

In order that Eq. (19) satisfies Eqs. (17) and (18) along the appropriate normal vectors, it is required that

$$\alpha + \beta \left(\frac{dy_s}{dx}\right)_{AP} = \frac{z_{AP}}{\delta_{AP}}$$

$$\alpha + \beta \left(\frac{dy_s}{dx}\right)_{F} = \frac{z_F}{\delta_F} \tag{21}$$

From Eqs. (6), if g_s and r are specified, dy_s/dx and consequently the z's are specified. Equations (20) and (21) are three equations in the four unknowns α, β, δ_{AP}, and δ_F. These may be computed uniquely if the heat transfer vector in the gas phase is specified.

If it is presumed that, as will be explained in more detail later, the gas phase temperature profile is represented by

$$g - g_s = (g_1 - g_s)\ f\left(\frac{y - y_s}{\delta_g - y_s}\right) \tag{22}$$

where $g_1 = g_1(s)$ is the temperature along a line $y = \delta_g$ in the gas phase and f is a function with the properties $f(0) = 0$, $f(1) = 1$, the interface heat transfer condition of Eqs. (6) may be computed. After some manipulation, an additional equation for α, β, δ_F, and δ_{AP} becomes

$$\frac{g_s'_{AP}\left(\frac{dy_s}{dx}\right)_{AP}}{z_{AP}} - \frac{g_s'_{F}\left(\frac{dy_s}{dx}\right)_{F}}{z_F} =$$

$$\xi\left\{\frac{q_{s_F}}{z_F^2} - \frac{q_{s_{AP}}}{z_{AP}^2} + \eta\left(g_s - 1\right)\left(\frac{1}{z_F\delta_F} - \frac{1}{z_{AP}\delta_{AP}}\right)\right\} \qquad (23)$$

where

$$g_s' = \left(g_s - 1\right)\left(-\frac{\alpha}{z} + \frac{\beta\,\frac{dy_s}{dx}}{z}\right)$$

is developed from Eq. (19).

A solution to Eqs. (20), (21), and (23) has been obtained with g_s and r as parameters at 800 psia and with $q_{s_F}^* = 77$ cal/gm. The results are shown in Fig. III-3. The equations are quadratic in the δ's and above a certain g_s, dependent upon r, no real solutions exist. In the region where real solutions exist, Fig. III-3 applies. The distressing thing about this figure is that g_{s_F}' is never negative which implies from Eq. (16) that the surface is convex.

It is at this point that some trouble may be anticipated in the solution of the sandwich problem by approximate methods. The assumed temperature profiles of Eqs. (17) and (18) may be highly inaccurate, and/or the assumed profile of Eq. (22), which gives a certain similarity of all temperature profiles in the y direction, may be highly in error.

E. Attempt at a Sandwich Solution

The overriding consideration in the analytical attempt was to avoid

a direct numerical integration because of the computer time anticipated with such a method for this complex nonlinear problem. Instead, an integral technique was formulated to simplify the problem while hopefully retaining the relevant physics. While many different approximate techniques were tried during the contract year, the method described below was the one settled upon as the most likely to give success with a minimum of computation.

The solid phase is most conveniently treated in the orthogonal curvilinear n, s coordinate system for which a differential element of length is

$$d\ell^2 = dn^2 + (1 + \kappa n)^2 ds^2$$

The transformation of Eq. (5) yields

$$\frac{\partial^2 g}{\partial n^2} + \frac{\kappa}{1 + \kappa n}\frac{\partial g}{\partial n} + \frac{1}{(1 + \kappa n)^2}\frac{\partial^2 g}{\partial s^2} + \frac{n\kappa'}{(1 + \kappa n)^3}\frac{\partial g}{\partial s}$$

$$= -\frac{1}{z}\frac{\partial g}{\partial n} + \frac{y_s'}{z^2}\frac{\partial g}{\partial s}\frac{1}{1 + \kappa n} \qquad (24)$$

The approach taken was a) to assume a temperature profile of the form of Eq. (17) with $\delta = \delta(s)$ and $g_s = g_s(s)$ and b) to use Eq. (24) evaluated at $n = 0$. This amounts to a collocation at the surface. The result is an ordinary differential equation for g_s.

$$g_s'' = \frac{(g_s - 1)}{\delta}\left(\frac{1}{z} + \kappa - \frac{1}{\delta}\right) + \frac{y_s' g_s'}{z^2} \qquad (25)$$

The reasons for this choice are as follows: a) the thermal profile matches exactly the required pure AP profile as $s \to -\infty$ for $\delta = z_{AP}$, b) the thermal profile yields the exact interface solution of Section D above, and c) the collocation at the interface eliminates terms in δ'', δ', and κ', which markedly simplifies the calculations. As $s \to -\infty$, the condition required is that $\delta \to z_{AP}$ and $\kappa \to 0$. From Eqs. (16) and (25) clearly $g_s'' \to 0$ even though y' is finite (θ_{AP} is nonzero).

The gas phase was treated in a more complex manner. Using the non-orthogonal curvilinear y, s system of coordinates, Eq. (4) becomes

$$\frac{\partial^2 g}{\partial y^2} + z^2 \frac{\partial^2 g}{\partial s^2} + z\kappa y_s' \frac{\partial g}{\partial s} = \xi \frac{\partial g}{\partial y} \tag{26}$$

As mentioned in Section B there is good reason for considering an elliptic problem totally imbedded within the y-direction scale required for completion of the AP flame. Consequently, a horizontal line located at $y = \delta_g$ which is of the order of $1/\xi$ is selected to bound the elliptic region. At $y = \delta_g$ the parabolic boundary condition is placed on Eq. (26) which says that the first term of Eq. (26) is negligible compared with the rest.

A profile of the form of Eq. (22) is then selected with $g_1 = g_1(s)$ as the temperature value on $y = \delta_g$. Equation (22) is placed in Eq. (26) and integrated over $y = y_s(s)$ to $y = \delta_g$. This amounts to a one strip integral method and yields an ordinary differential equation in g_1 and g_s as follows:

$$g_1'' = (1 - 1/\beta)\, g_s'' + \frac{1}{z^2\left[\beta(\delta_g - y_s) + 1/\xi\right]} \left\{\left[\xi + \frac{\alpha z^2}{(\delta_g - y_s)} + \beta\kappa z^3\right] \times \right.$$

$$\left[g_1 - g_s\right] + y_s' \left[1 - \kappa z(\delta_g - y_s)\right]\left[g_s' + \beta(g_1' - g_s')\right]$$

$$\left. + \beta y_s'(g_1' - g_s') - y_s'\, g_s' - \frac{g_1' z\kappa y_s'}{\xi}\right\} \tag{27}$$

where the parabolic condition has been used in generating Eq. (27) and

$$\alpha = \left.\frac{df(\tilde{y})}{d\tilde{y}}\right]_{\tilde{y}\,=\,0} \qquad\qquad \beta = \int_0^1 f(\tilde{y})\, d\tilde{y}$$

Once the profile function f is chosen Eq. (27) is determined. For a linear temperature profile $\alpha = 1$, $\beta = \frac{1}{2}$; for an exponential $\alpha = 0.58$, $\beta = 0.42$.

The basic reason for use of this procedure is that Eq. (27) is already quite complex. The use of more complex temperature profiles to allow dissimilar behavior in y at different s positions would require further generation of more ordinary differential equations since more unknowns than merely g would be introduced. Similarly, the use of more than one strip would introduce more unknowns and require the introduction of more differential equations.

The link between the gas and the solid phases comes about through the interface heat transfer condition of Eqs. (6). Using the assumed gas and solid phase thermal profiles

$$\frac{(g_1 - g_s)\alpha z}{\delta_g - y_s} - \frac{y_s'}{z} g_s' = \xi\left[\frac{q_s}{z} + \frac{\eta(g_s - 1)}{\delta}\right] \tag{28}$$

The integration procedure used was the following:

a) Assume values for r, $g_s(s = 0)$, and $g_1'(s = 0)$.

b) At the starting point, s = 0 values are found for z_F and z_{AP} at the interface from Eqs. (6), the pyrolysis laws.

c) δ_F, δ_{AP}, g_{s_F}', and $g_{s_{AP}}'$ at the interface are found through the procedure of Section D.

d) $g_1(0)$ is found from Eq. (28).

e) $\varkappa$ is found from Eq. (16).

f) Integration of Eqs. (25) and (28) may then proceed if at each step $\varkappa$ is found from Eq. (16), z from the pyrolysis laws, and δ from Eq. (28).

The boundary conditions are

$$g_1 \to g_s \quad \text{as} \quad y_s \to \delta_g$$

$$\delta \to z_{AP} \quad \text{as} \quad s \to -\infty$$

$$\varkappa \to 0 \quad \text{as} \quad s \to -\infty$$

The integration proceeds along positive s until y is within ϵ of δ_g and then from s = 0 an integration is performed through negative s to some distance greater than $1/\xi$. The errors in the quantities g_1, δ, and $\varkappa$ are noted and a systematic variation of the guessed quantities is begun to start a convergence scheme.

This scheme requires that the pure AP deflagration is reached at negative s before the line $y = \delta_g$ intersects the AP flame, because no chemical reaction is included in Eq. (27). The adjustment distance is open to some doubt because the solid phase can only adjust in distance scales of the order of unit y, while the gas phase adjusts over distances of the order of $1/\xi$. If $\theta_{AP} > 0$, then clearly as $s \to -\infty$ the AP flame will be penetrated by the line $y = \delta_g$. To this time $s = -\infty$ has been defined to be at distances of the order of a few $1/\xi$ units from the origins, so that this problem has not arisen.

The distressing point is that to this time the procedure does not yield a solution. This is a two point, nonlinear boundary value problem with an eignenvalue r. There is mathematically no guarantee of a solution. However, the original partial differential equations should yield a physically meaningful solution, on physical grounds. Unless the physics have been so distorted with the approximate method of solution, it would be anticipated that a solution would exist because experimentally one does exist.

There are several things which could be wrong, and these will be examined. First, the profile choices were shown in Section D to yield an unrealistic interface condition when compared with experiment. The use of more complex profiles in the solid phase, however, negates the possibility of a simple analytical solution in this vicinity. The use of more complex profiles in either the gas or solid phases increases the number of required differential equations. If the number of differential equations increase the algebraic complexity mounts, computer time soars, and the problem is compounded when chemical reaction and the attendant mass fraction equations are considered. The gas phase temperature profile is especially suspect, but if more strips in y were considered, the solution could be made as accurate as desired. But each strip introduces a new differential equation to which the above objections are raised. Second, the presumption of a pyrolysis law

for AP may be constraining the solution and forcing the unrealistic interface condition. However, physically a solution should exist to the problem as formulated. Third, the region bounds employed, artificially imposing the parabolic condition at $y = \delta_g$, may be at fault. It is clearly in error as one proceeds toward the pure AP deflagration in regions of strong y gradients. As the binder is approached, the approximation should be adequate. This condition, coupled with the potential inadequacy of gas phase profiles is considered one of the weakest points in the analysis. Fourth, there could be errors in the computer program, of course.

Assuming that the last cause is not dominant, the question remains in future work as to what direction to take. It may readily be shown that the shape of the sandwich, in the case of no contribution from the BO flame, is dependent upon the nature of the ignition transient. For uniform ignition the slope of the AP should be horizontal, away from the binder. It is first recommended that a one strip integral method be used, abandoning the parabolic condition, to investigate the allowable solutions for the pure AP to relax to a horizontal state. A more sophisticated analysis of the solid phase heat transfer condition in the interface vicinity should then be performed. Work is currently under way in these two areas. If it becomes apparent that the integral techniques are requiring too much sophistication to yield a solution, it is recommended that a direct numerical integration be attempted, or at least a study of the difficulty of such an attempt should be made. This represents a formidable task, and there is real question concerning the probability of success using a reasonable amount of computer time. Nevertheless, the interpretation difficulty of the experimental results warrants continued attempts at analytical modeling.

IV. SUMMARY AND CONCLUSIONS

In this combined experimental-analytical program several areas in cinephotomacrography of sandwiches were tied together and conclusions drawn concerning real propellant behavior. The analytical work, while not completely successful, was able to point to certain critical relationships which must hold in sandwich combustion and thereby aid in interpretation of experimental results.

A rather complete catalogue over the pressure range 600-3200 psia has been obtained for compacted polycrystalline AP sandwiches using PU, PBAA, CTPB, and HTPB sandwiches. With the exception of some anomolous "Christmas tree" profiles obtained in the 2000-28000 psia range, which are probably related to the AP behavior, there is evidence that the binder plays little role in the deflagration rate of sandwiches at pressures above the low pressure deflagration limit of pure AP. The behavior in the vicinity of the binder oxidizer interface, however, is dominated by the binder melts and possibly binder-oxidizer chemical reactions.

The insensitivity of the gross sandwich behavior to the presence of the binder changes, however, when catalysts are added. In this program IO and CC catalysts were investigated with HTPB-AP sandwiches over the pressure range 600-3200 psia. HTPB behaves quite similarly to CTPB in these catalyzed situations as it also does in uncatalyzed sandwiches. The evidence is clear that with both catalysts there is a dominant effect near the interface, which includes the binder behavior and which increases with pressure, that causes the leading edge of regression to take place near the interface. This effect is stronger if the catalyst is either pressed with the AP or coated on the AP at the interface; it is virtually absent if the catalyst is in the binder. The exact nature of this effect, whether it is a purely gas phase phenomena or involves heterogeneous attack upon the binder, can best be determined by

future quenched-combustion photomicroscopy work. A conclusion drawn from this work concerning actual propellant behavior is that catalyst effectiveness should become greater, the smaller the oxidizer size, if the method of catalyst addition is by mixing with the binder. Furthermore, ways should be sought to introduce the catalyst directly into the AP or on the AP surface.

Copper chromite was found to augment the pure AP deflagration rate at all pressures and to become most effective in augmenting the interface phenomena above 2000 psia. Iron oxide retarded the pure AP below 1000 psia, augmented it above 1000 psia, but augmented the interface phenomena at all pressures, the augmentation increasing with pressure.

The addition of aluminum to the binder makes no gross difference in the regression history, and the cinephotomacrography used here did not have the resolution to detect agglomeration. This does not preclude, however, the use of sandwiches for Al studies with high resolution methods. The study of AN and KP sandwiches did not prove fruitful. The highly mobile melt on KP during combustion made a highly erratic flame. AN proved difficult to work with and difficult to ignite.

Order of magnitude analyses indicate that heat transfer processes adjust on quite disparate distance scales and that there is reason to suspect that, in accord with the experimental conclusion, binder oxidizer reactions do not substantially affect the interface behavior for uncatalyzed situations. The interface in these situations should be dominated by the heat transfer from the hot AP decomposition gases, fed by the AP flame, and only a short distance from the interface, compared to the thermal wave depth in the solid, the binder should be consumed by a boundary layer flow, which may contain a diffusion flame. A highly approximate model based upon these concepts was constructed but a solution to the sandwich deflagration problem was not obtained. The numerical difficulties most probably have their origin in distortion of physics due to the approximations.

The sandwich technique has proved especially valuable in the screening of catalysts. In order to resolve the nature of the interface behavior it is recommended that quenched combustion tests be initiated so that the interface may be viewed with high resolution. Furthermore, additional catalysts should be studied with both cinephotomacrography and quenched combustion tests. The goal of an analytical model of sandwich combustion should be pursued as a potentially valuable aid in interpretation of experiments. This goal may most likely be achieved by systematically removing the approximations or by returning to solution of the original partial differential equations.

LIST OF CAPTIONS

Figure III-3 Solution to the interface heat transfer model

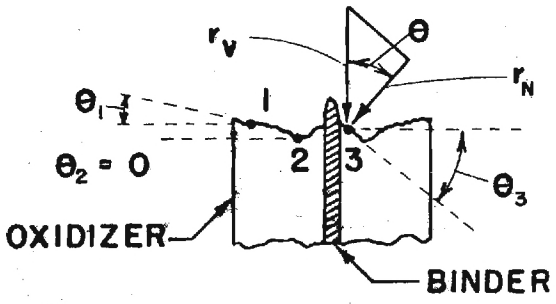

$$r_V = \frac{r_N}{\cos \theta} \qquad r_{V1} = r_{V2} = r_{V3} = \text{CONSTANT}$$

$$\theta_3 > \theta_1 > \theta_2 \Rightarrow r_{N2} > r_{N1} > r_{N3}$$

(a) REGRESSION ANALYSIS MODEL

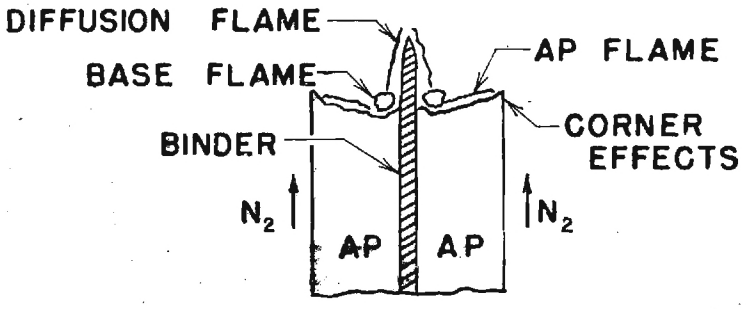

(b) COMBUSTION MODEL

Figure II-1

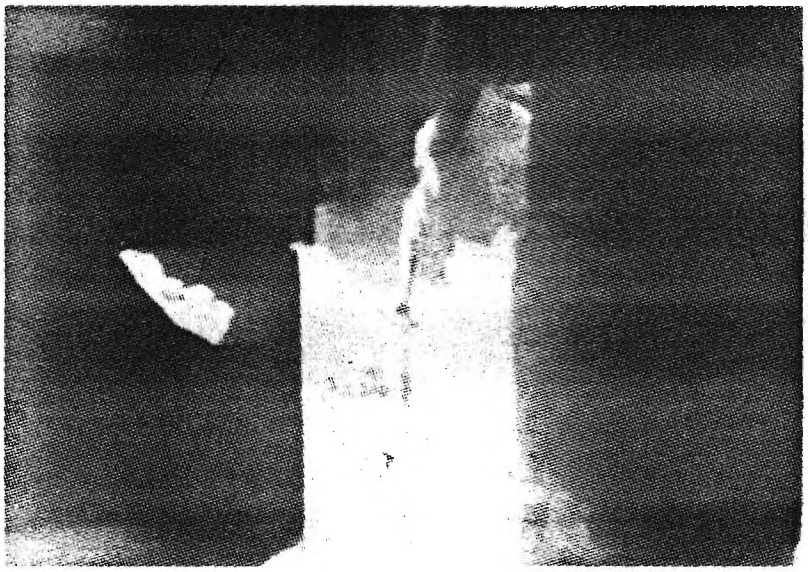

Figure II-2

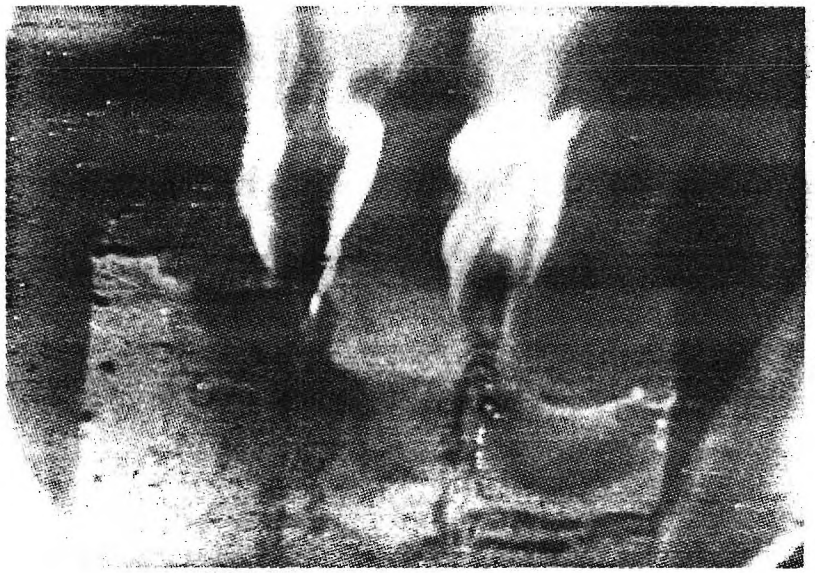

Figure II-3

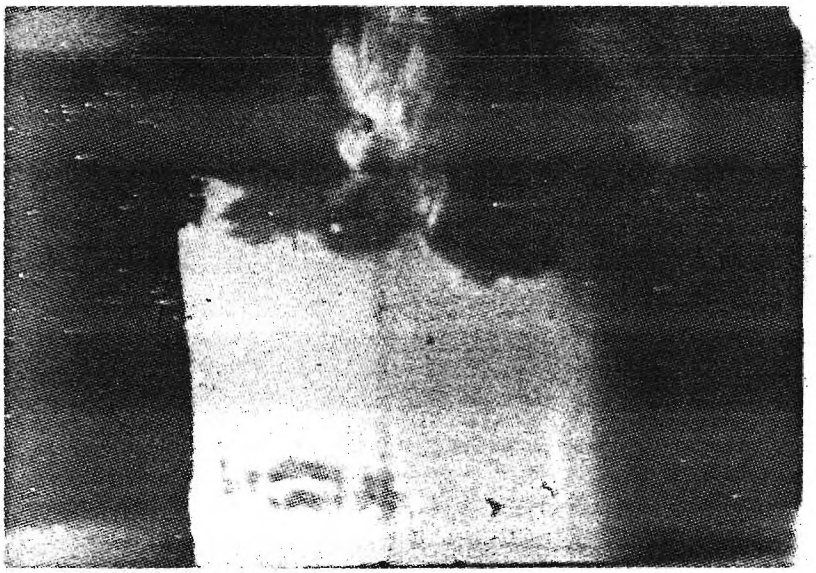

Figure II-4

Figure II-5

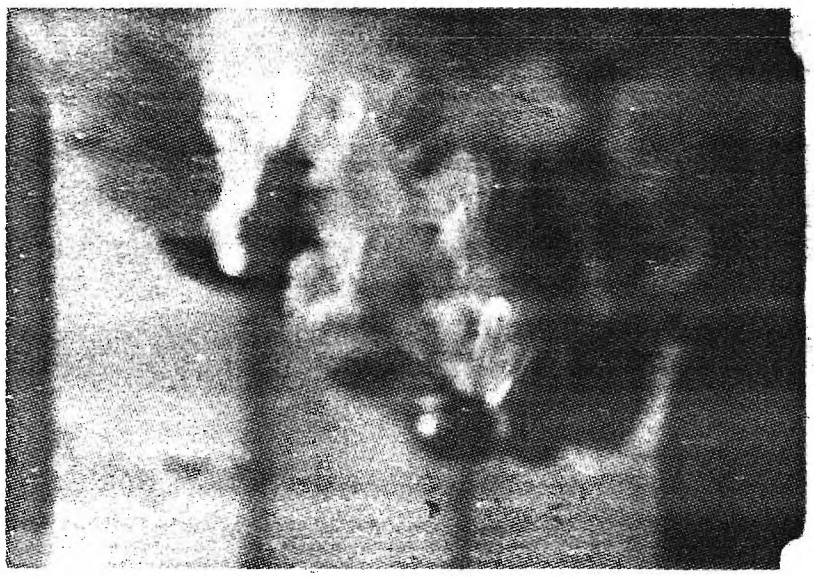

Figure II-6

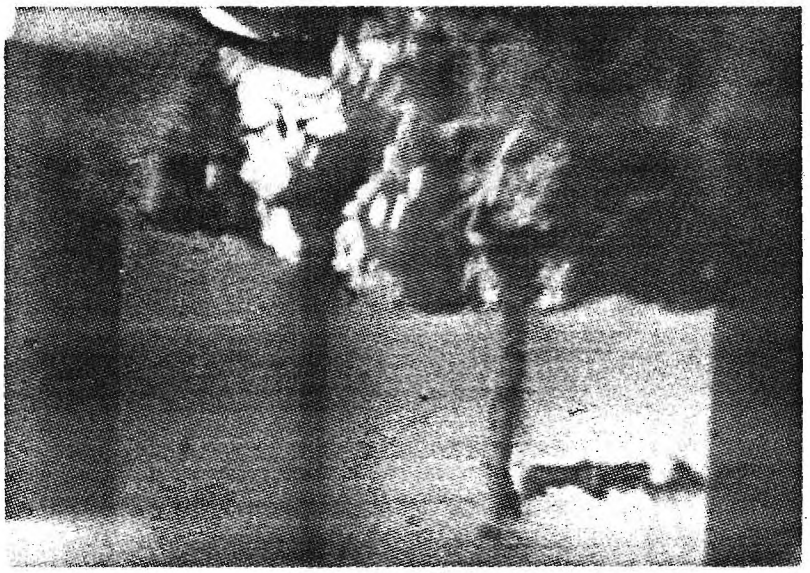

Figure II-7

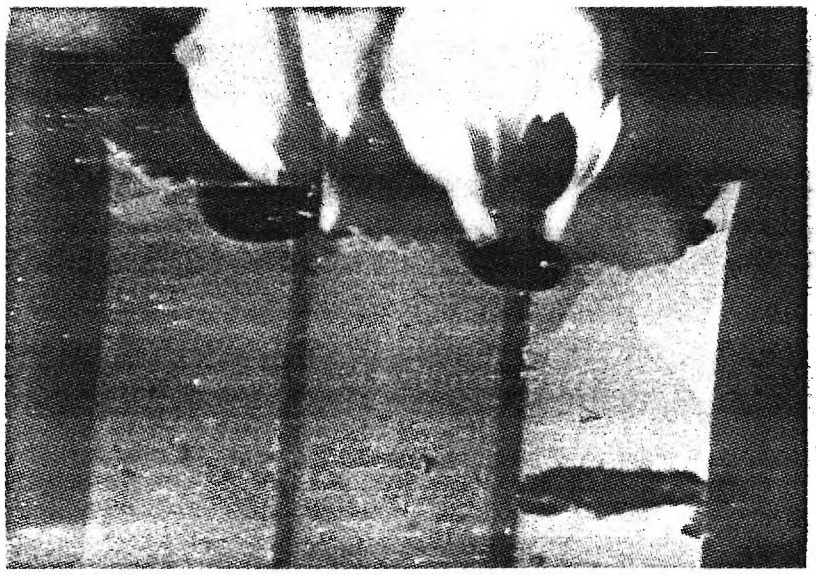

Figure II-8

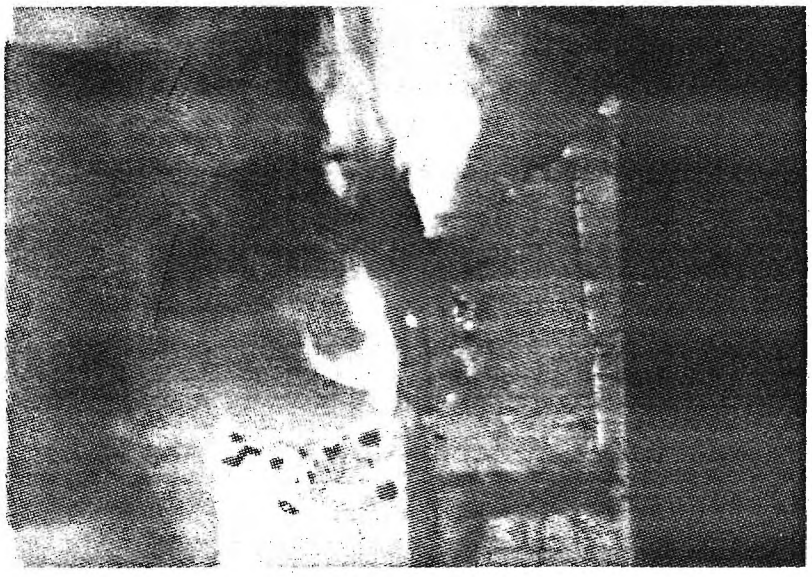

Figure II-9

Figure II-10

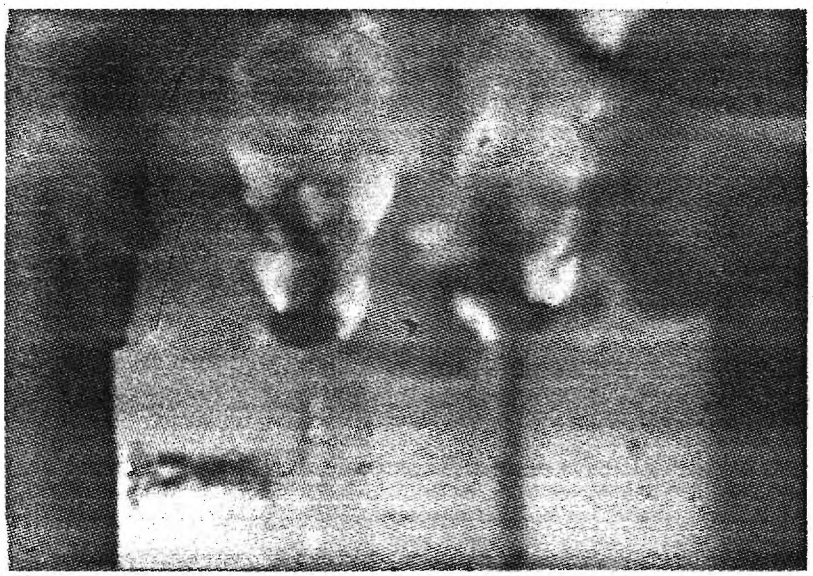

Figure II-11

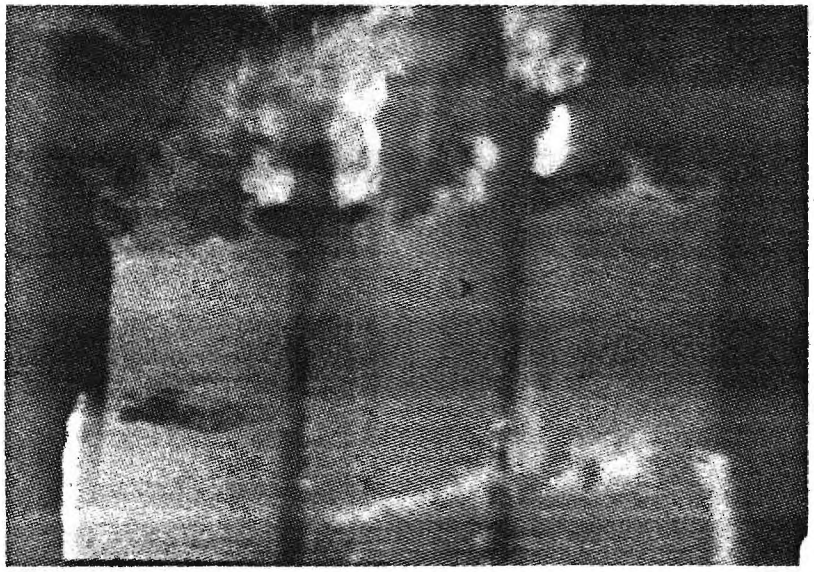

Figure II-12

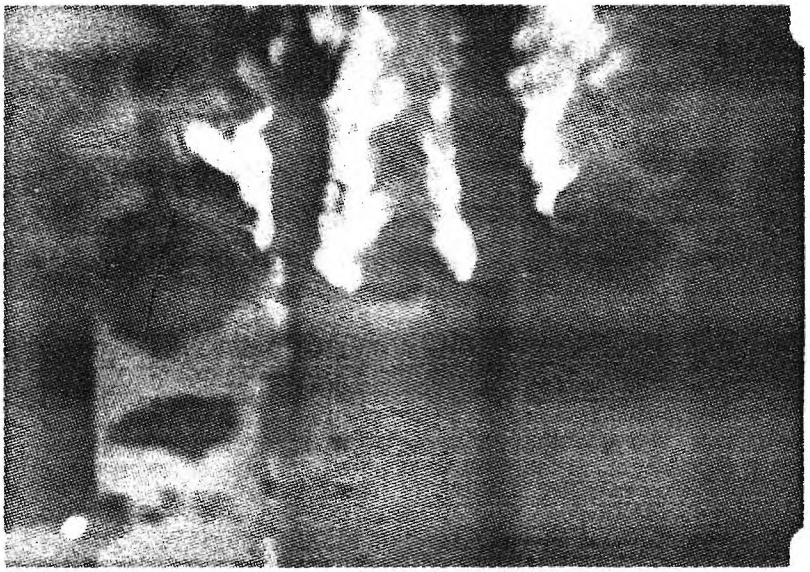

Figure II-13

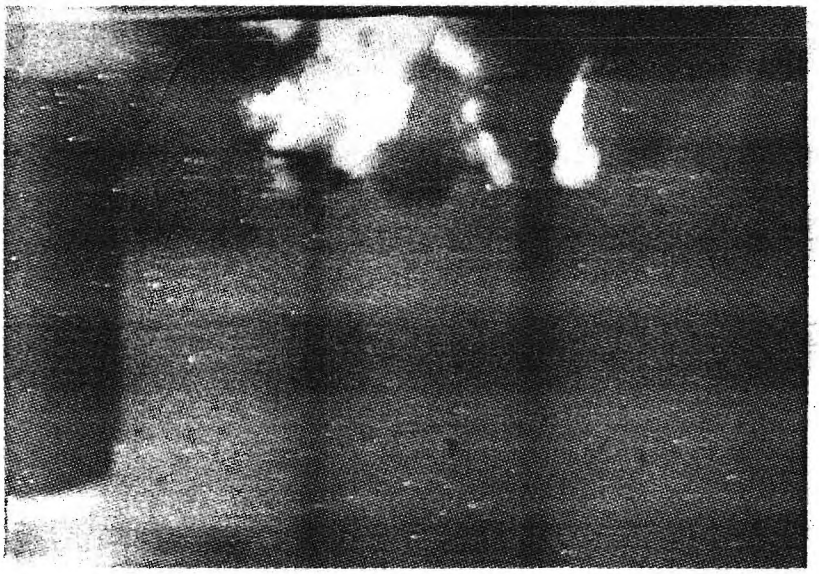

Figure II-14

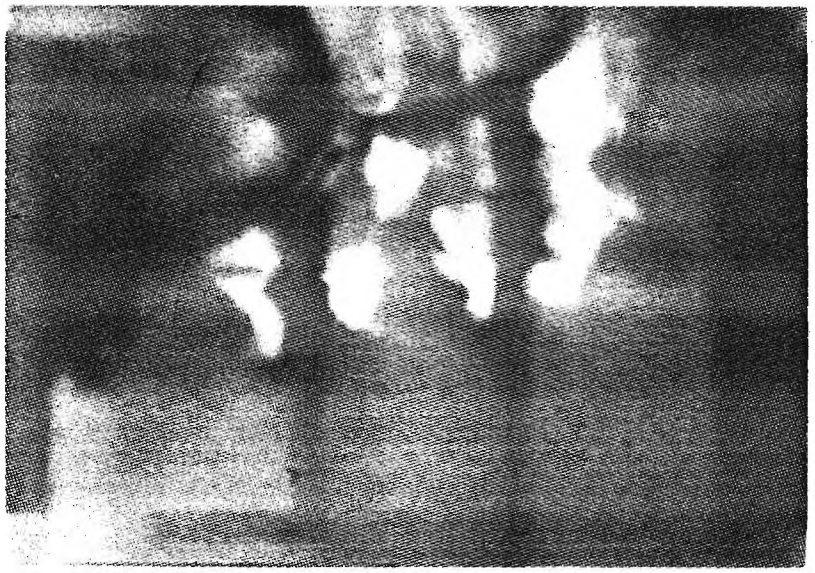

Figure II-15

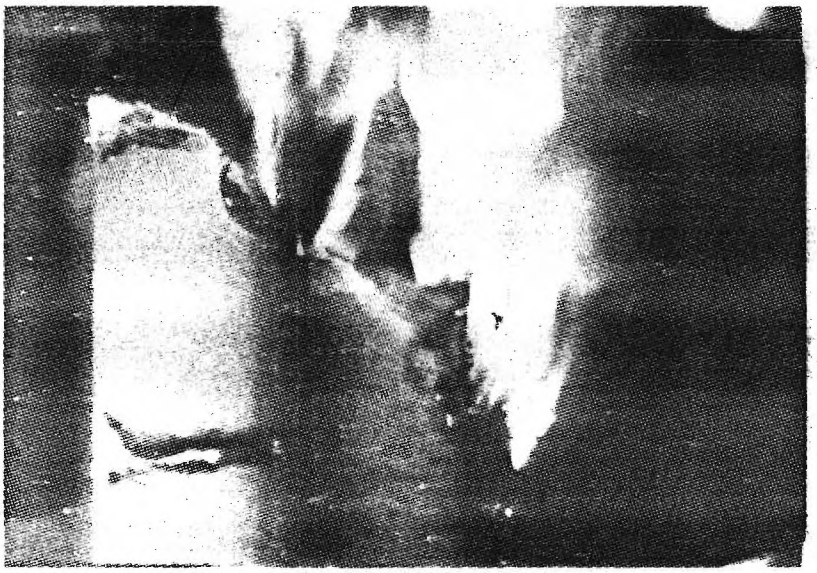

Figure II-16

Figure II-17

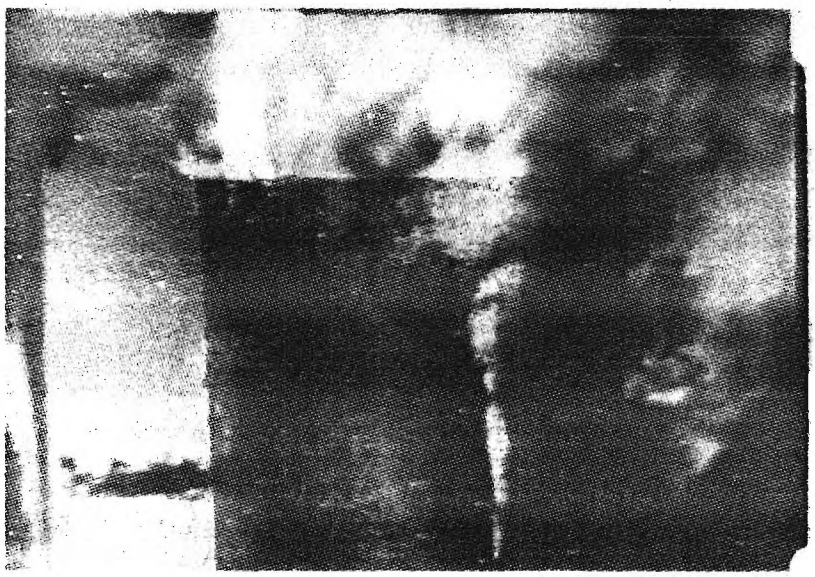

Figure II-18

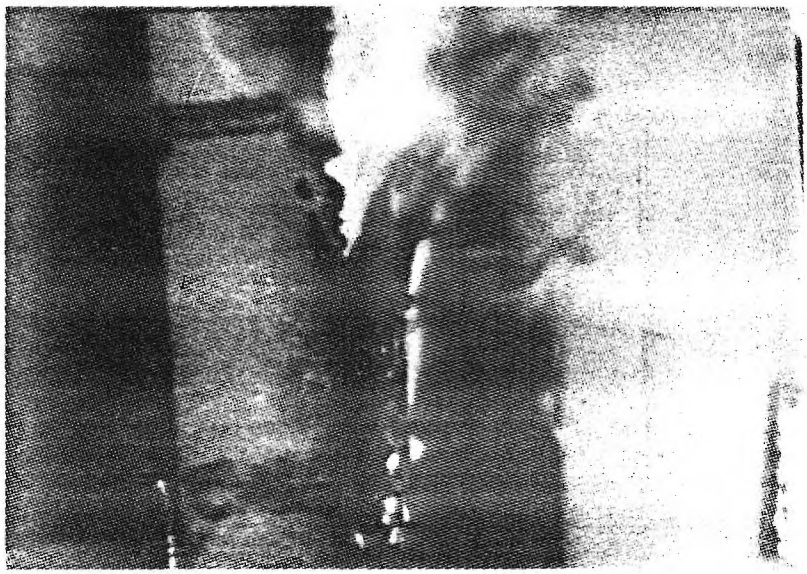

Figure II-19

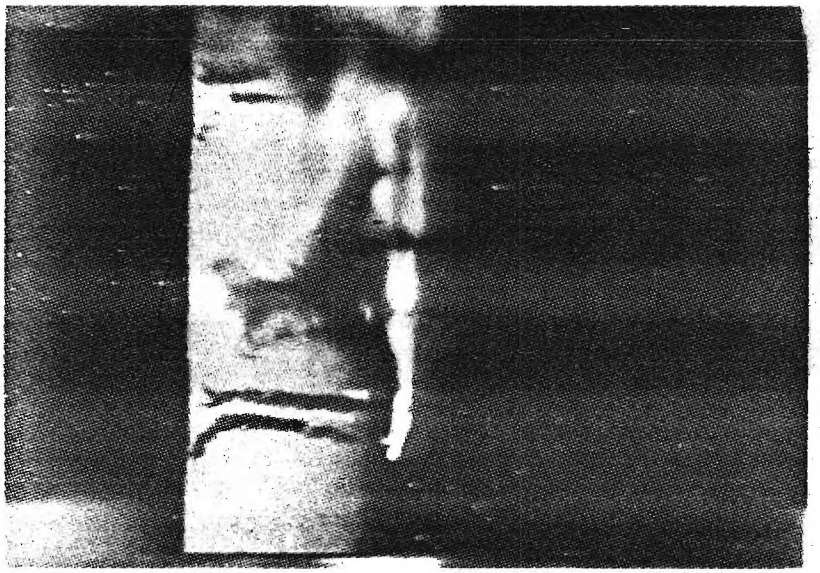

Figure II-20

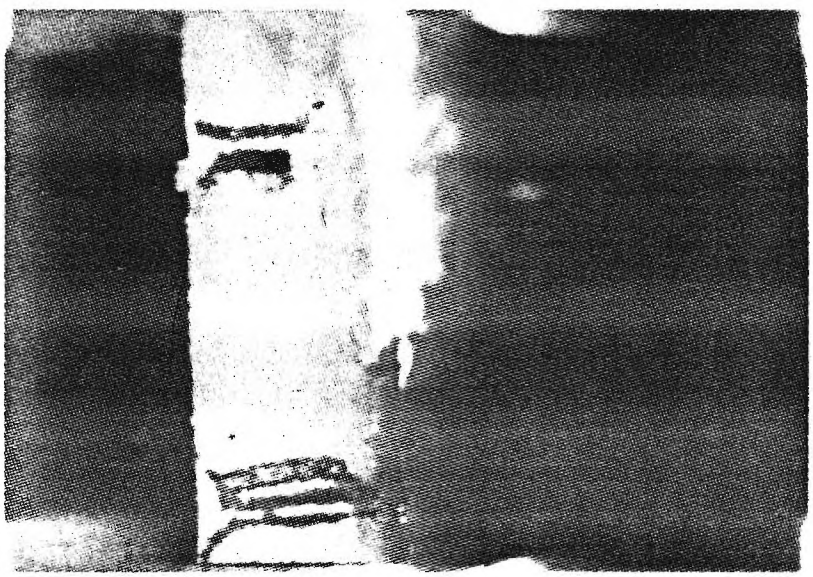

Figure II-21

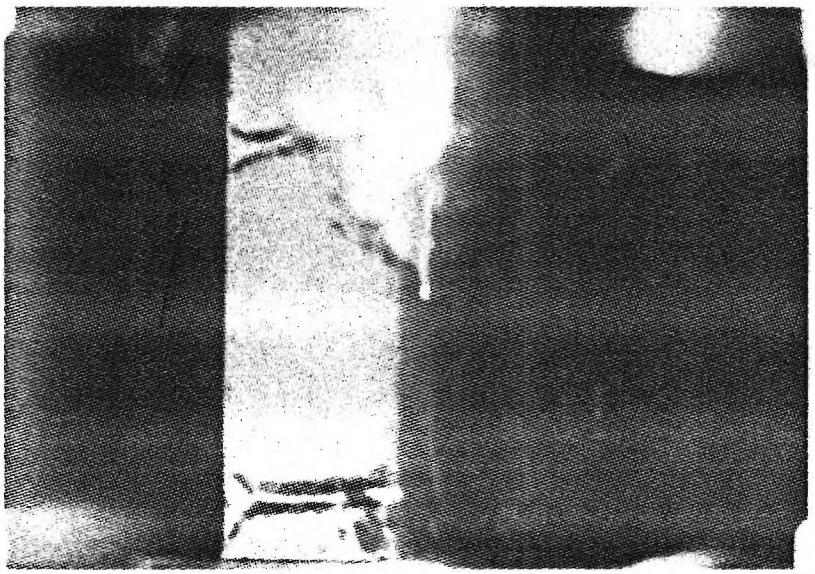

Figure II-22

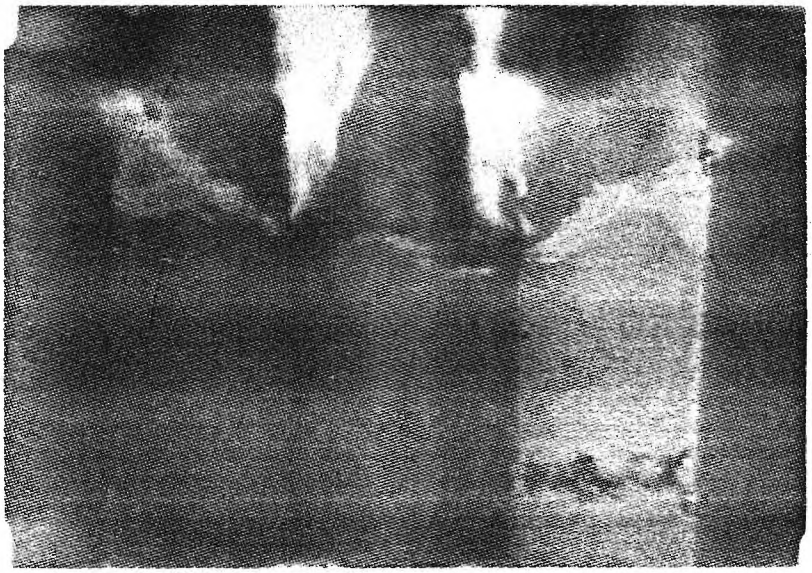

Figure II-23

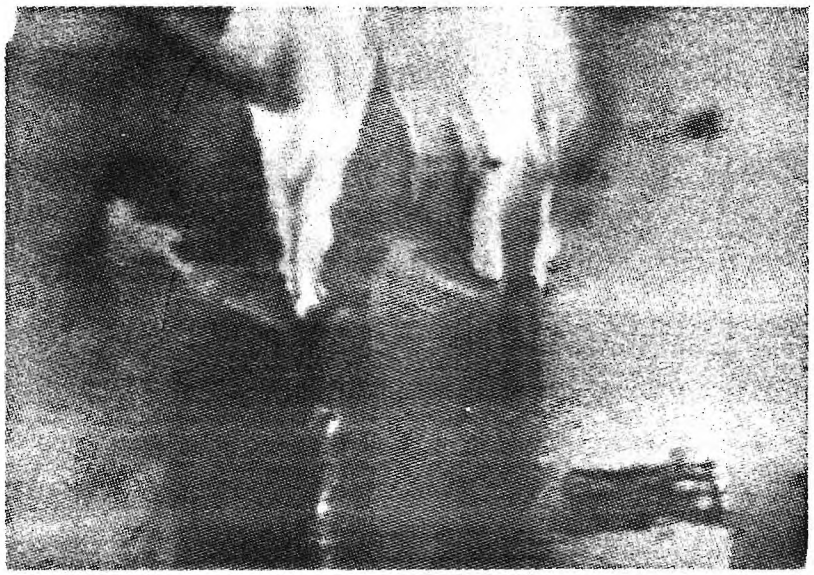

Figure II-24

Figure II-25

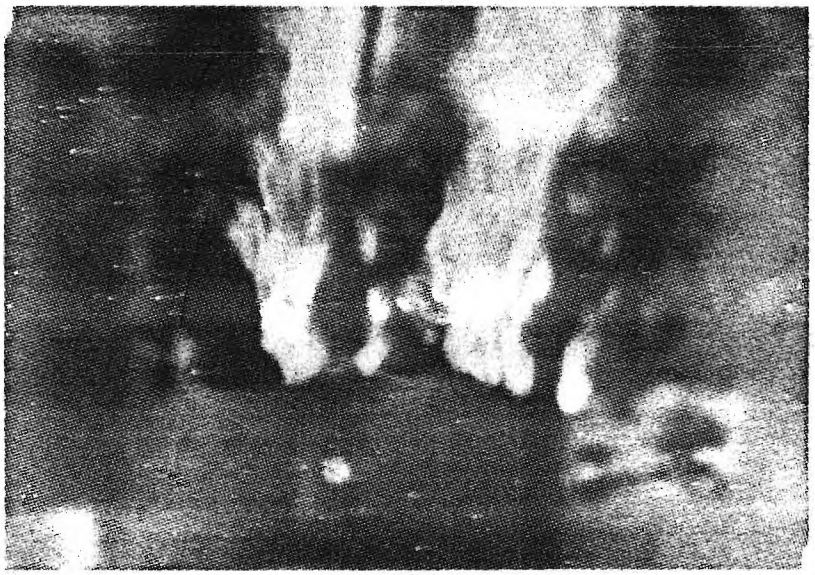

Figure II-26

Figure II-27

Figure II-28

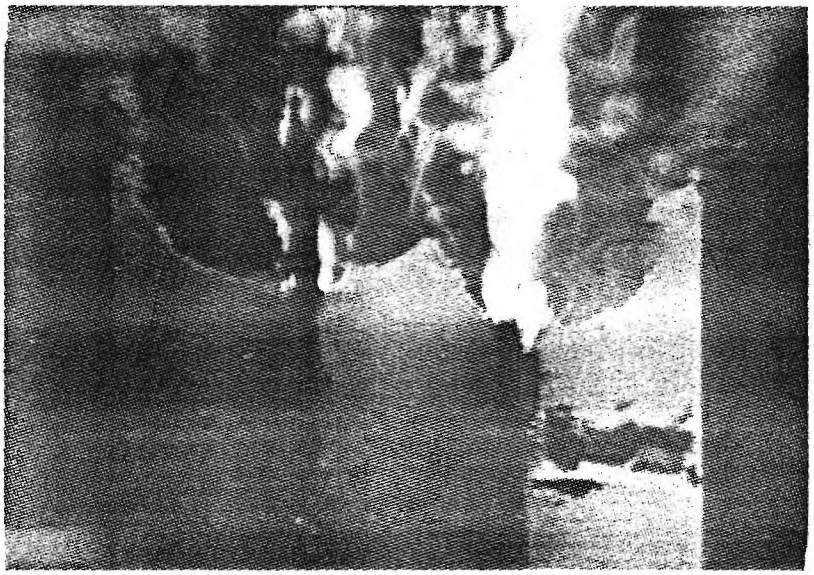

Figure II-29

Figure II-30

Figure II-31

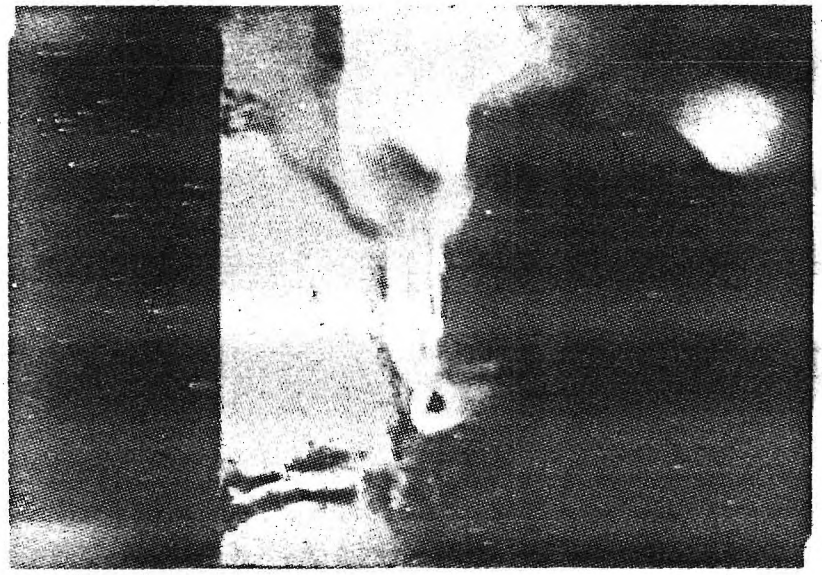

Figure II-32

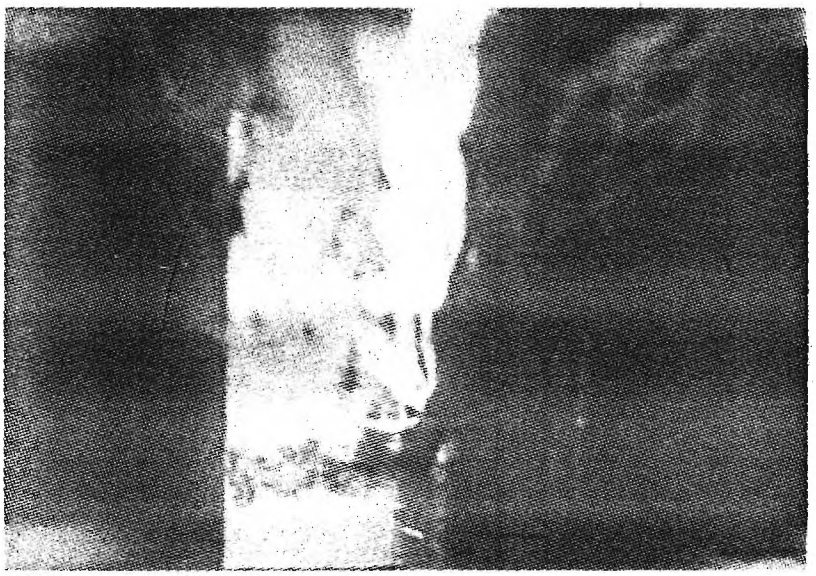

Figure II-33

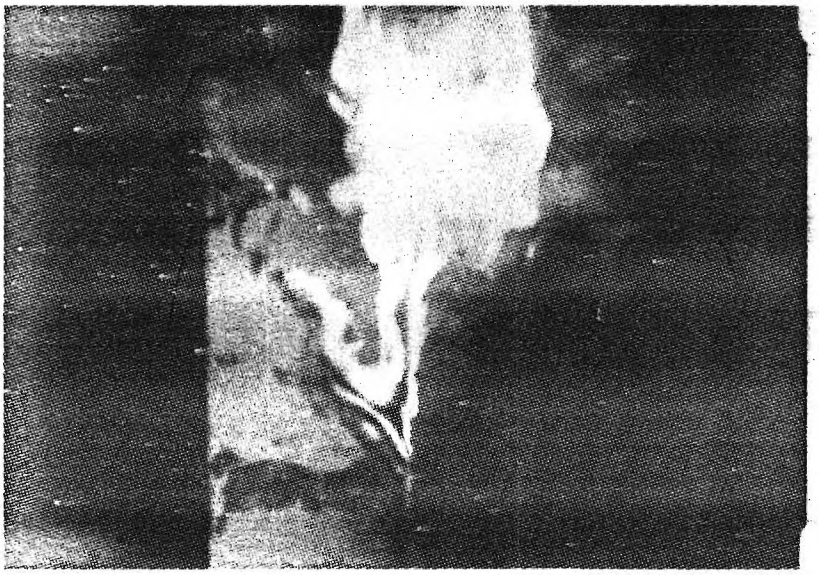

Figure II-34

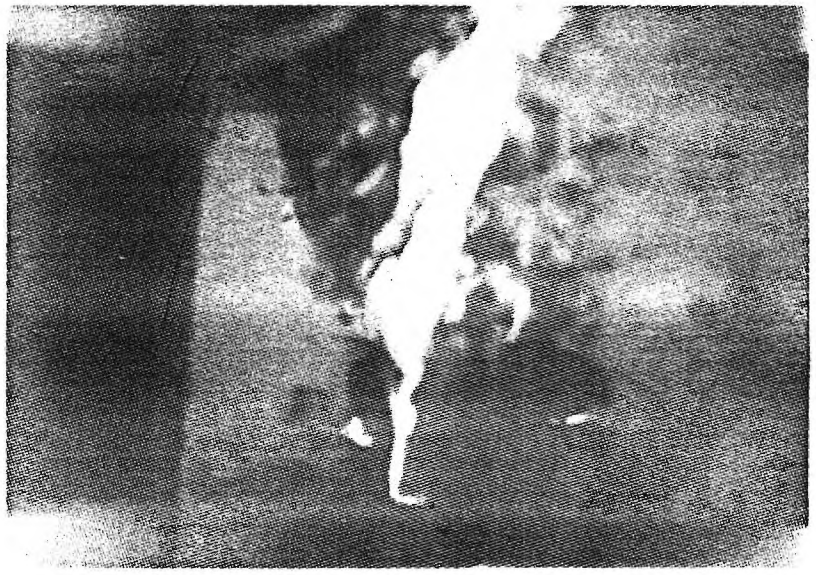

Figure II-35

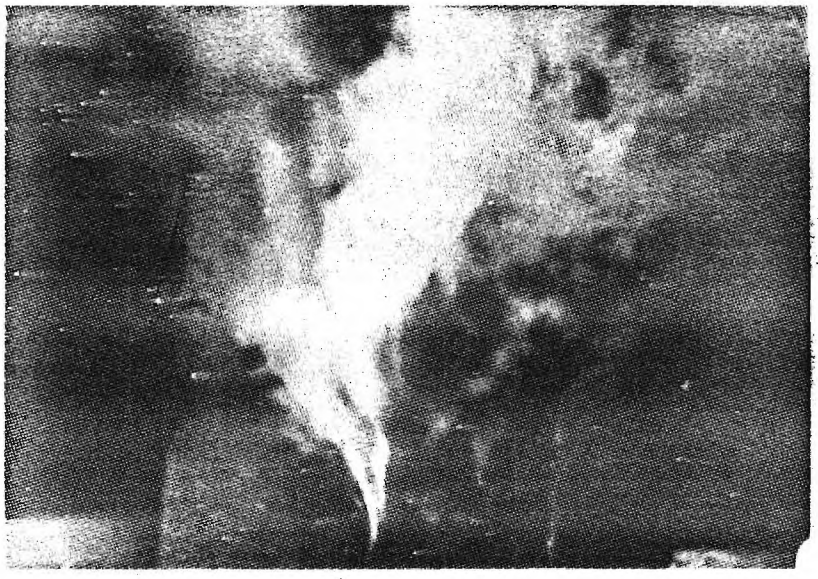

Figure II-36

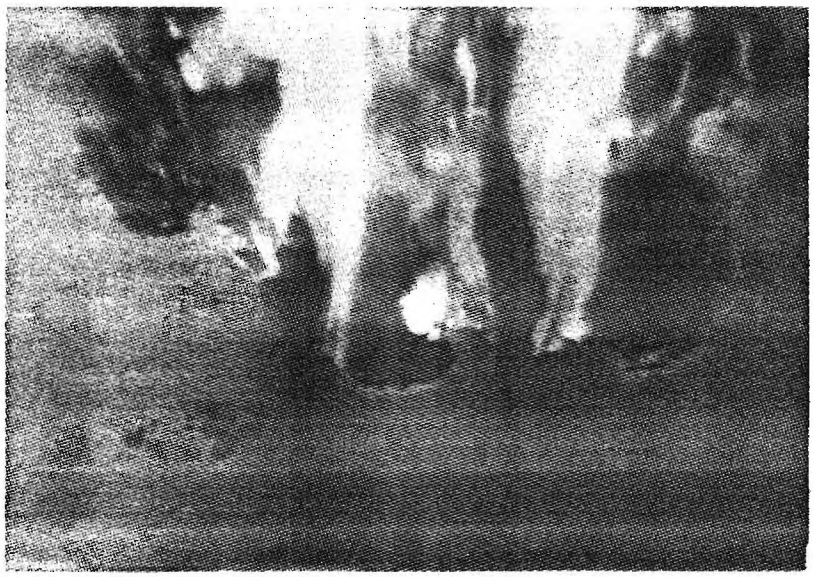

Figure II-37

Figure II-38

Figure II-39

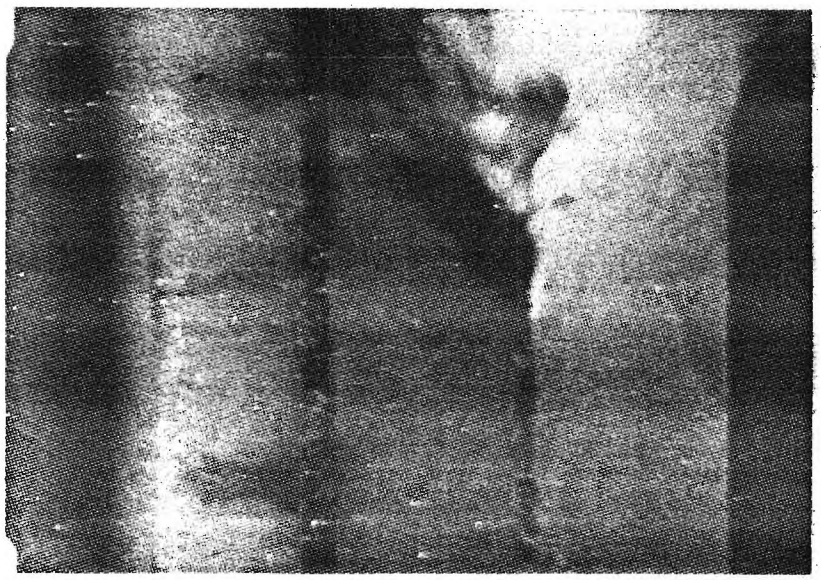

Figure II-40

Figure II-41

Figure II-42

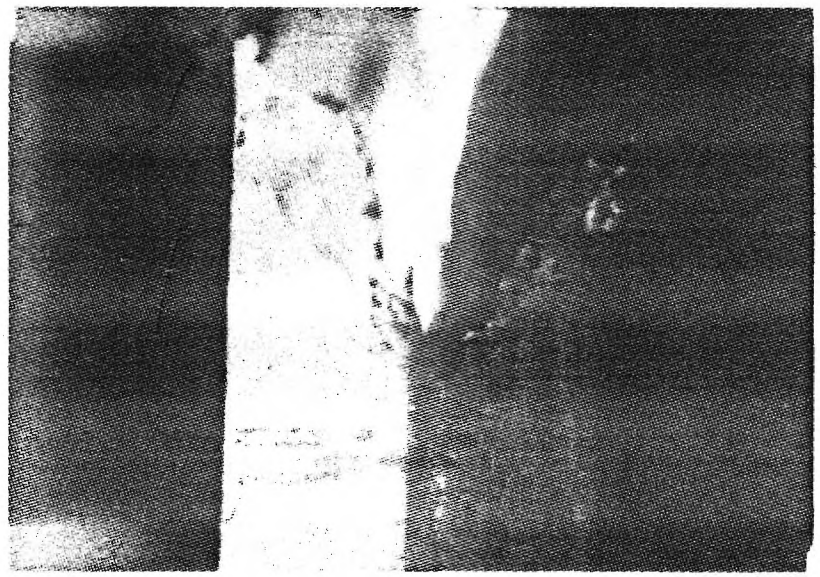

Figure II-43

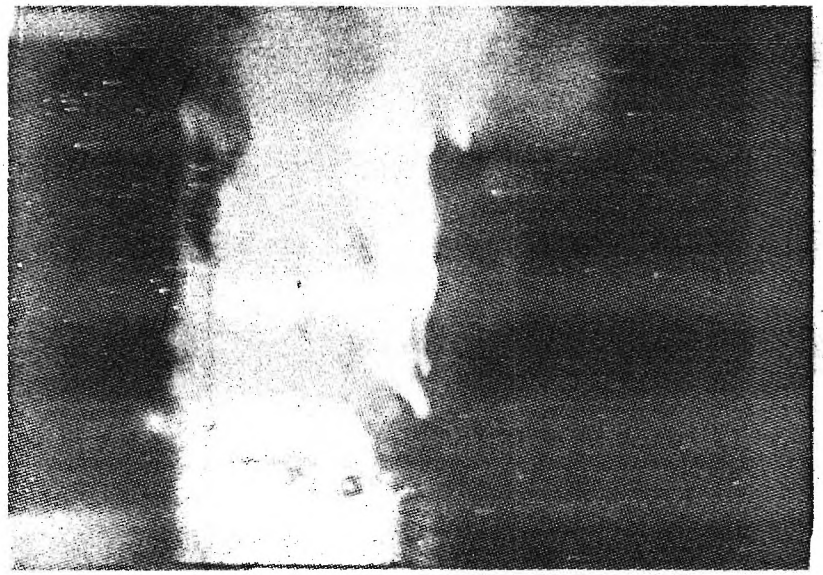

Figure II-44

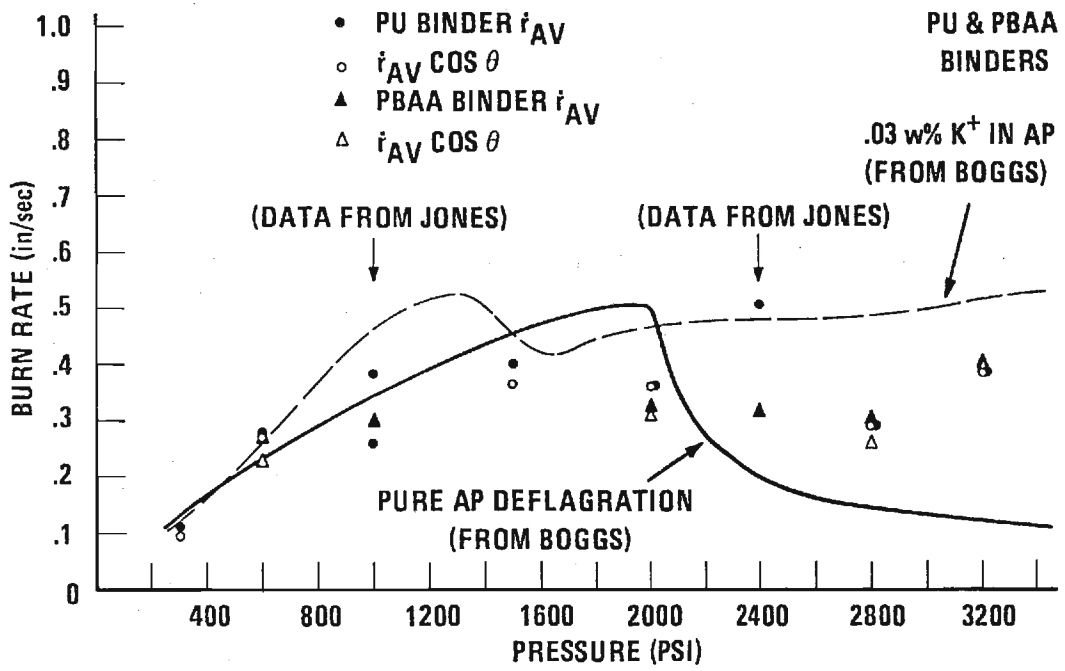
PU BINDER r_{AV}
r_{AV} COS θ
PBAA BINDER r_{AV}
r_{AV} COS θ
PU & PBAA BINDERS
.03 w% K^+ IN AP (FROM BOGGS)
(DATA FROM JONES)
(DATA FROM JONES)
PURE AP DEFLAGRATION (FROM BOGGS)
BURN RATE (in/sec)
1.0
.9
.8
.7
.6
.5
.4
.3
.2
.1
0
400
800
1200
1600
2000
2400
2800
3200
PRESSURE (PSI)

Figure II-45

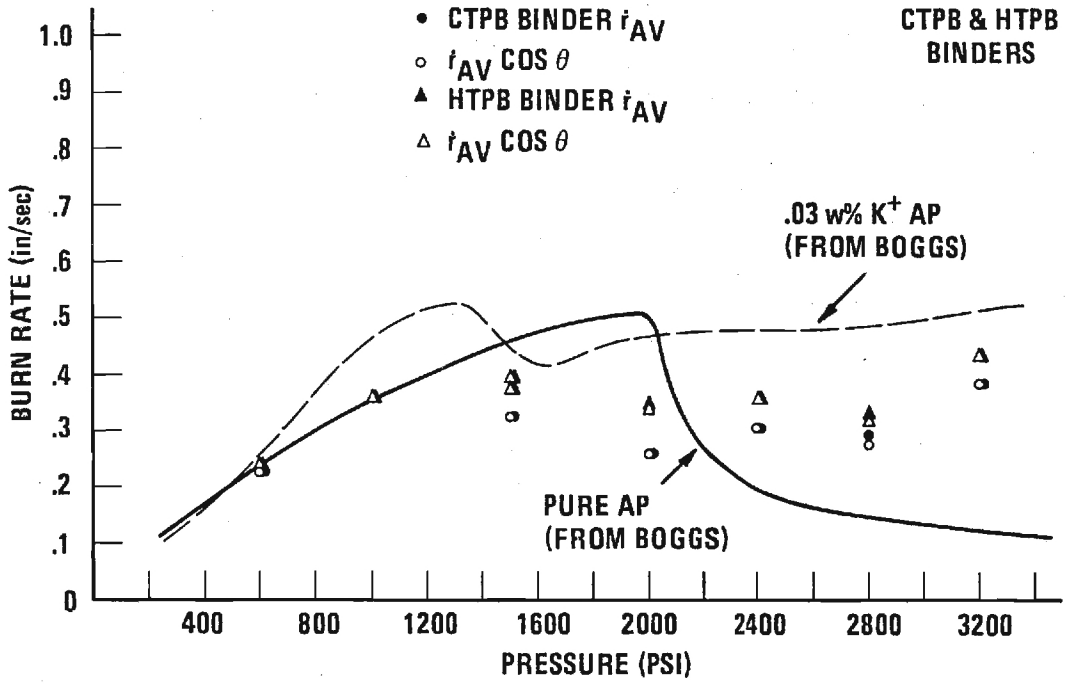
• CTPB BINDER $\dot{r}_{AV}$
○ $\dot{r}_{AV}$ COS θ
▲ HTPB BINDER $\dot{r}_{AV}$
△ $\dot{r}_{AV}$ COS θ
CTPB & HTPB BINDERS
.03 w% K^+ AP (FROM BOGGS)
PURE AP (FROM BOGGS)
BURN RATE (in/sec)
1.0
.9
.8
.7
.6
.5
.4
.3
.2
.1
0
400
800
1200
1600
2000
2400
2800
3200
PRESSURE (PSI)

Figure II-46

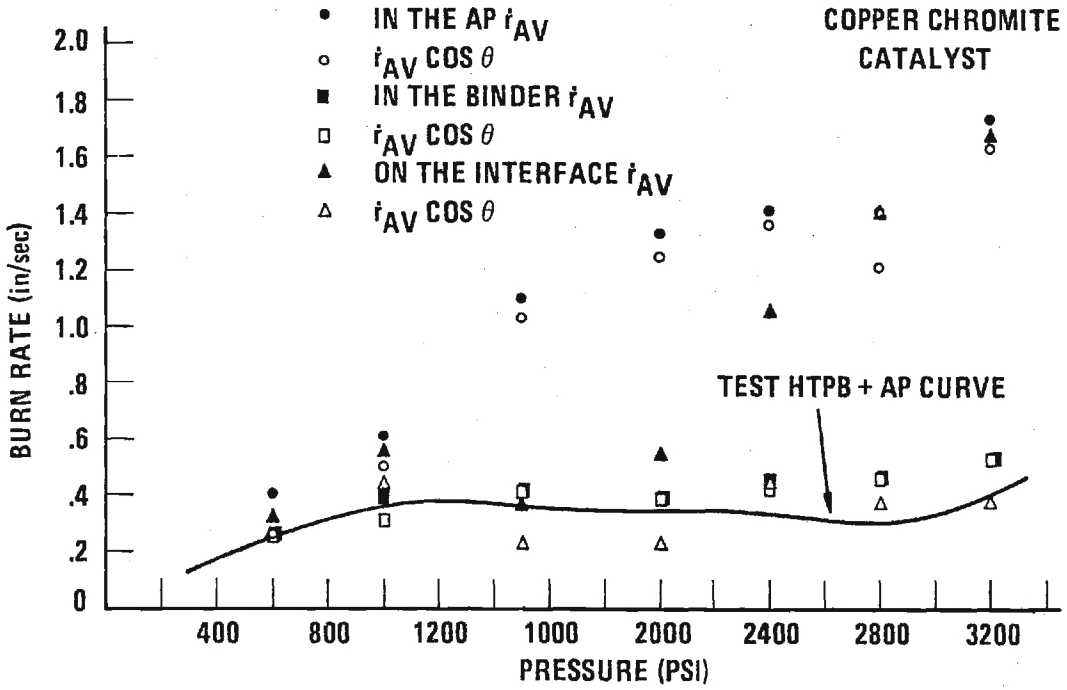
IN THE AP i_{AV}
i_{AV} COS θ
IN THE BINDER i_{AV}
i_{AV} COS θ
ON THE INTERFACE i_{AV}
i_{AV} COS θ
COPPER CHROMITE CATALYST
TEST HTPB + AP CURVE
BURN RATE (in/sec)
2.0
1.8
1.6
1.4
1.2
1.0
.8
.6
.4
.2
0
400
800
1200
1000
2000
2400
2800
3200
PRESSURE (PSI)

Figure II-47

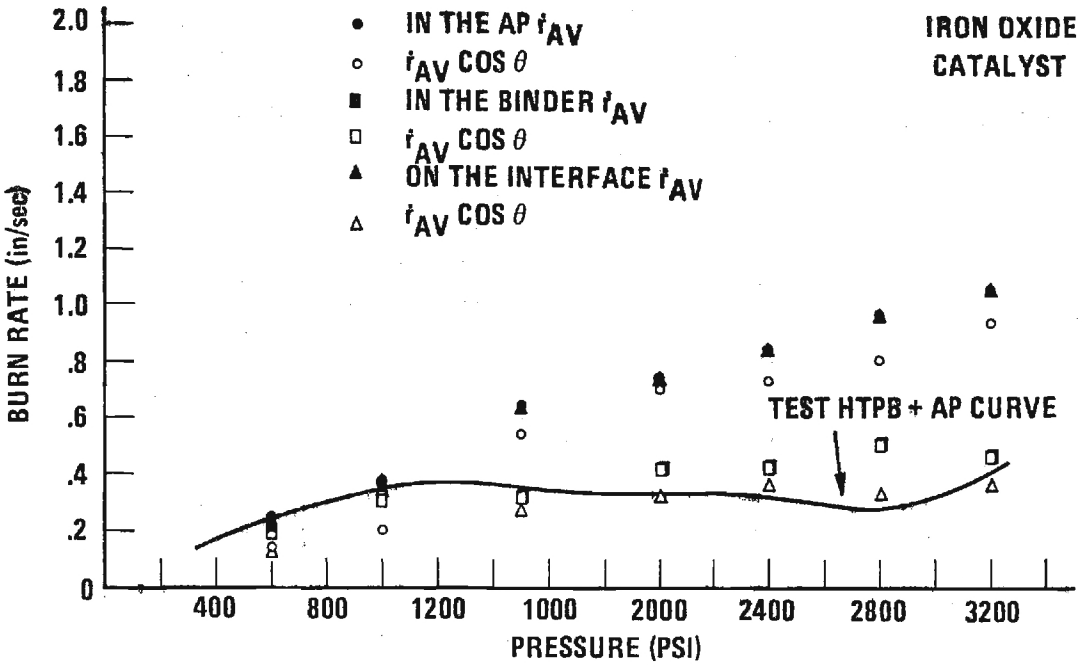
IRON OXIDE
CATALYST
IN THE AP r_{AV}
r_{AV} COS θ
IN THE BINDER r_{AV}
r_{AV} COS θ
ON THE INTERFACE r_{AV}
r_{AV} COS θ
TEST HTPB + AP CURVE
BURN RATE (in/sec)
2.0
1.8
1.6
1.4
1.2
1.0
.8
.6
.4
.2
0
400
800
1200
1000
2000
2400
2800
3200
PRESSURE (PSI)

Figure II-48

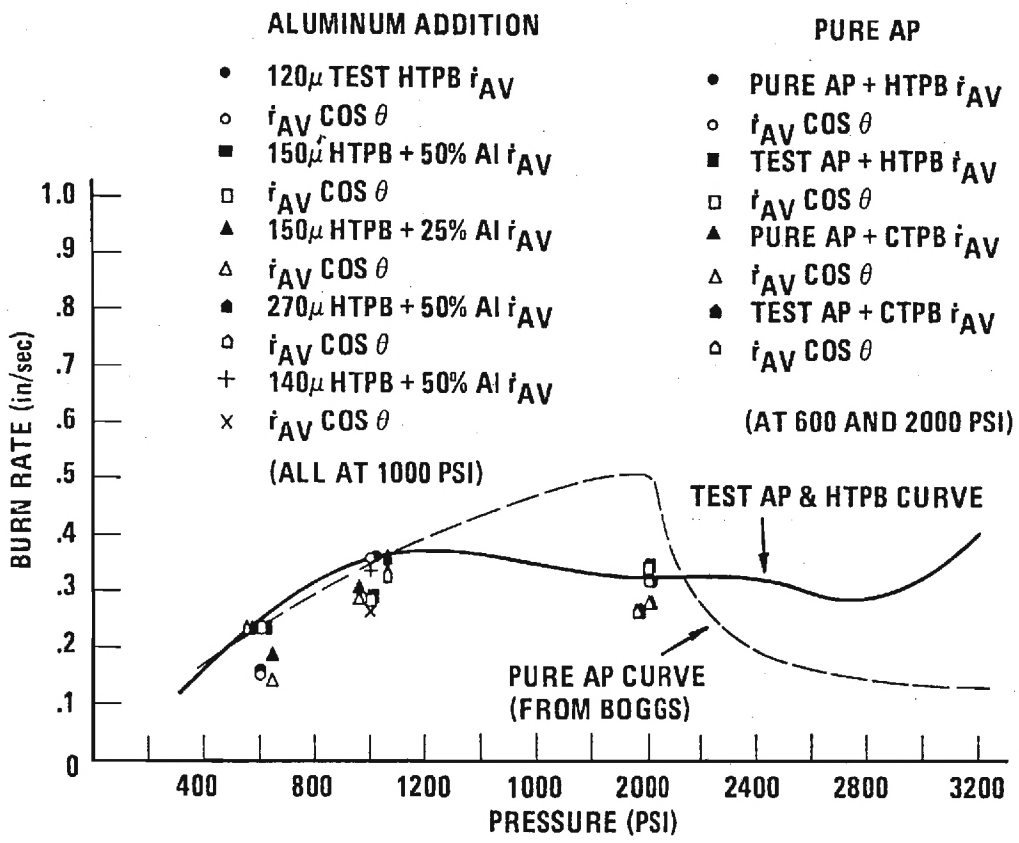
ALUMINUM ADDITION
• 120μ TEST HTPB i_{AV}
○ i_{AV} COS θ
■ 150μ HTPB + 50% Al i_{AV}
□ i_{AV} COS θ
▲ 150μ HTPB + 25% Al i_{AV}
△ i_{AV} COS θ
⬟ 270μ HTPB + 50% Al i_{AV}
⌂ i_{AV} COS θ
+ 140μ HTPB + 50% Al i_{AV}
× i_{AV} COS θ
(ALL AT 1000 PSI)
PURE AP
• PURE AP + HTPB i_{AV}
○ i_{AV} COS θ
■ TEST AP + HTPB i_{AV}
□ i_{AV} COS θ
▲ PURE AP + CTPB i_{AV}
△ i_{AV} COS θ
⬟ TEST AP + CTPB i_{AV}
⌂ i_{AV} COS θ
(AT 600 AND 2000 PSI)
TEST AP & HTPB CURVE
PURE AP CURVE
(FROM BOGGS)
BURN RATE (in/sec)
1.0
.9
.8
.7
.6
.5
.4
.3
.2
.1
0
400
800
1200
1000
2000
2400
2800
3200
PRESSURE (PSI)

Figure II-49

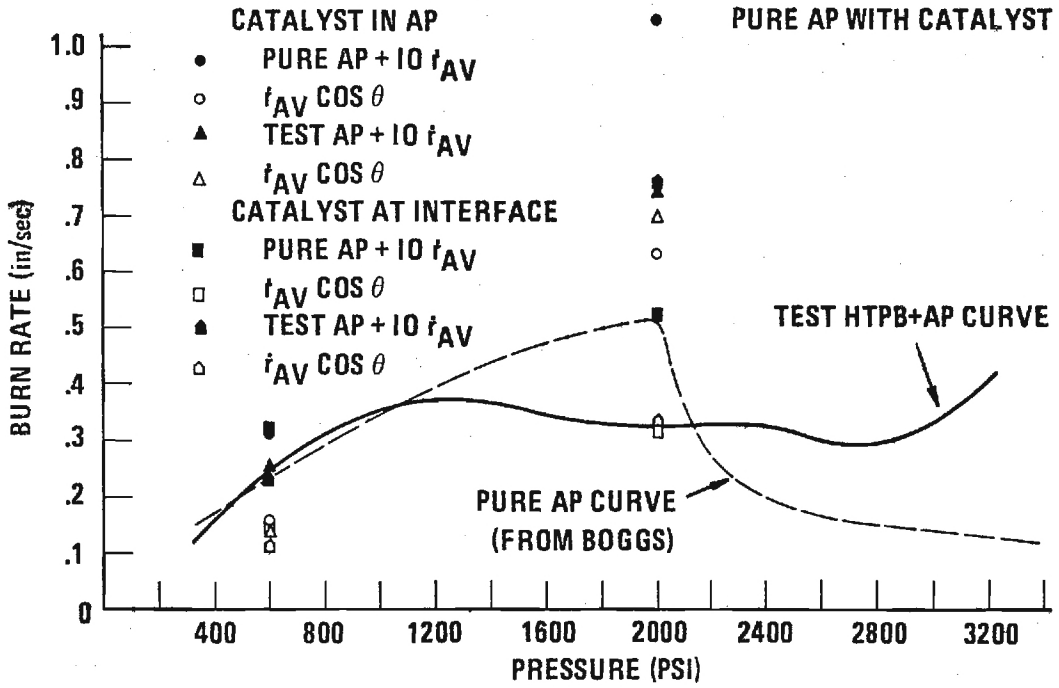
CATALYST IN AP
PURE AP + 10 t_{AV}
t_{AV} COS θ
TEST AP + 10 t_{AV}
t_{AV} COS θ
CATALYST AT INTERFACE
PURE AP + 10 t_{AV}
t_{AV} COS θ
TEST AP + 10 t_{AV}
t_{AV} COS θ
PURE AP WITH CATALYST
TEST HTPB+AP CURVE
PURE AP CURVE
(FROM BOGGS)
BURN RATE (in/sec)
1.0
.9
.8
.7
.6
.5
.4
.3
.2
.1
0
400
800
1200
1600
2000
2400
2800
3200
PRESSURE (PSI)

Figure II-50

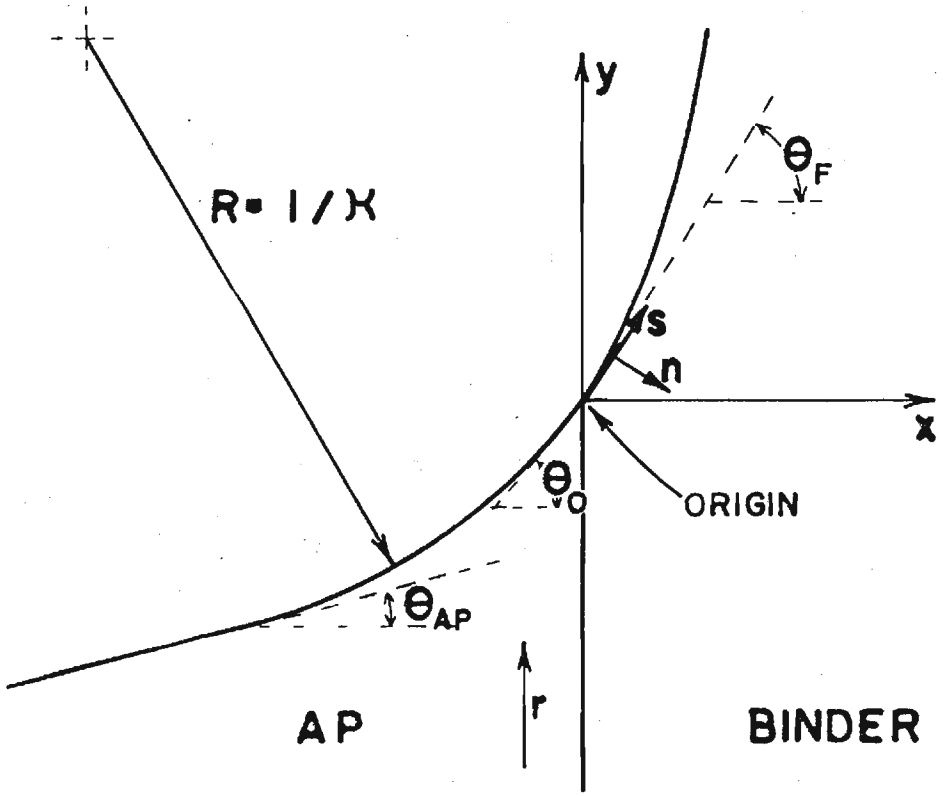

Figure III-1

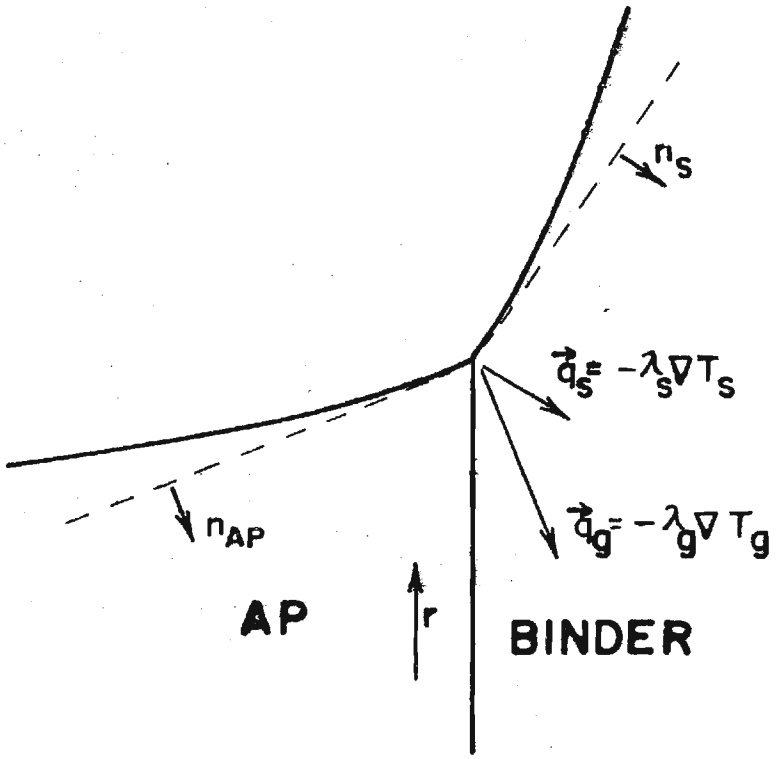
n_s
$\vec{q}_s = -\lambda_s \nabla T_s$
n_{AP}
$\vec{q}_g = -\lambda_g \nabla T_g$
AP
r
BINDER

Figure III-2

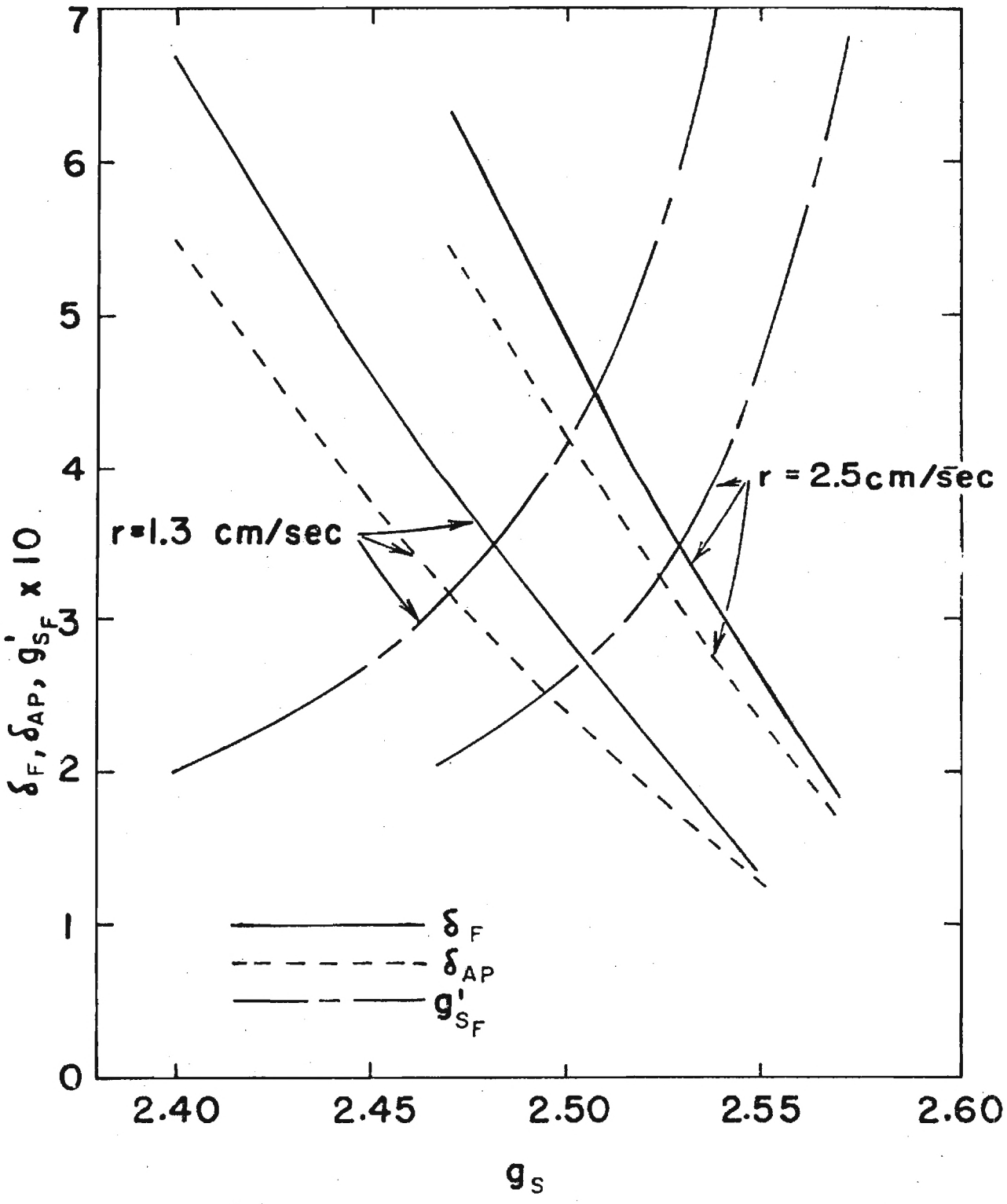
7
6
5
4
3
2
1
0
2.40
2.45
2.50
2.55
2.60
g_S
$\delta_F, \delta_{AP}, g'_{S_F} \times 10$
r=1.3 cm/sec
r = 2.5cm/sec
δ_F
δ_{AP}
g'_{S_F}

Figure III-3

REFERENCES

1. Nadaud, L. 1968 Combustion and Flame, 12, 177.
2. Powling, J. 1965 ERDE Report No. 15-R-65, Waltham Abbey, Essex.
3. Austin, T. D. 1967 Fourth ICRPG Combustion Conference, CPIA Publication No. 162, Vol. 1
4. Hightower, J. D. and Price, E. W. 1968 Astronautica Acta, 14.
5. Varney, A. M. 1970 Ph.D. Dissertation, Georgia Institute of Technology.
6. Jones, H. E. 1971 Ph.D. Dissertation, Georgia Institute of Technology.
7. Boggs, T. L. and Zurn, T. E. 1972 Combustion Science and Technology, 4, 279.
8. Fenn, J. B. 1968 Combustion and Flame, 12.
9. Boggs, T. L., Price, E. W., and Zurn, D. E. 1970 Naval Weapons Center NWC TP 4981.
10. Pearson, G. S. 1970 Combustion and Flame, 14, 73.
11. Pearson, G. S. and Sutton, D. 1967 AIAA J., 5, 344.
12. Derr, R. L. 1971 7th JANNAF Combustion Meeting, CPIA Publication No. 204.
13. Nachbar, W. 1960 in Progress in Astronautics and Rocketry, Vol. 1 - Solid Propellant Rocket Research (Martin Summerfield, ed.), New York: Academic Press.
14. Guirao, C. and Williams, F. A. 1971 AIAA J., 9, 1345.
15. Williams, F. A. 1965 Combustion Theory, 37, Reading, Mass.: Addison-Wesley.
16. Myers, B. F. and Bartle, C. R. 1969 AIAA J., 7, 1862.
17. Bakhman, N. N. and Librovich, V. B. 1970 Combustion and Flame, 15, 143.
18. Culick, F. E. C. and Dehority, G. L. 1969 Combustion Science and Technology, 1, 193.
19. Strahle, W. C. 1971 AIAA J., 9, 565.